NUMERICALLY MODELING THE FLOW AND FRICTION WITHIN A
HELICALLY-FINNED TUBE

by

James Shuster

Submitted in Partial Fulfillment of the Requirements

for the Degree of

Master of Science

in the

Mechanical Engineering

Program

YOUNGSTOWN STATE UNIVERSITY

May 2010

NUMERICALLY MODELING THE FLOW AND FRICTION WITHIN A
HELICALLY-FINNED TUBE

By

James Shuster

I hereby release this thesis to the public. I understand that this thesis will be
made available from the OhioLINK ETD Center and the Maag Library Circulation
Desk for public access. I authorize Youngstown State University or other
individuals to make copies of this thesis as needed for scholarly research.

Signature:

James Shuster	Date

Approved:

Dr. Hazel Marie, Thesis Advisor	Date

Dr. Daniel H. Suchora, Committee Member	Date

Dr. Yogendra M. Panta, Committee Member	Date

Dr. Peter Kasvinsky, Dean of Graduate Studies & Research	Date

ABSTRACT

As the populations and the economies of the world grow, the demand for electricity rises and necessitates an increase in the supply of electricity as the primary fuels that are used to generate electricity are finite and exhausting. Moreover, mounting concerns about carbon emissions and the current direction of environmental legislation are pushing for lower emissions and higher efficiencies of energy producing facilities. One approach to abate such dilemmas is to increase the efficiency of the modern steam cycle, which is used to generate most of the world's electricity. Improving the components of the steam cycle, or the boiler component in particular, can affect the overall efficiency of the steam cycle significantly. An integral constituent of the boiler is the boiler tube. There are several types of boiler tubes, and the helically-finned tube is one type that has proven to increase the efficiency of the boiler. However, insight to the internal flow within the helically-finned tube is still developing and incomplete. The objective of this study was to computationally model the internal flow and measure the friction factor of a helically-finned tube for which experimental data was already published. Using three different modeling techniques, the flow was solved numerically with Fluent, a computational fluid dynamics software package. With respect to the experimental data, the Fluent solutions reflected percent errors ranging between 14% and 27%. Although the results are acceptable, suggestions for future work are included.

ACKNOWLEDGEMENTS

TABLE OF CONTENTS

Page

LIST OF TABLES

LIST OF FIGURES

NOMENCLATURE

A	Surface area (m^2)
c_p	Specific heat at constant pressure (J/kg-K)
C	Constant used in Nusselt number correlation
$C_{(\ )}$	k-ε model constants
D	Diameter (m)
D_h	Hydraulic Diameter
e	Fin height (m)
e^*	Roughness Height
e^+	Roughness Reynolds number
f	Fanning friction factor
G	Heat transfer roughness function
h	Convective heat transfer coefficient (W/m^2-K)
H	Pitch for 180° roatation of twisted tape (m)
H_R	Helix ratio
j	Colburn j-factor (=StPr$^{2/3}$)
k	Thermal conductivity (W/m-K)
l_c	Characteristic length (m)
l_{csw}	Modified characteristic length for swirling flows (m)
L	Length of the tube (m)
$\vec{L}$	Periodic length vector

$\dot{m}$	Mass flow rate (kg/s)
N_{faces}	Number of faces
N_s	Number of fin starts
Nu	Nusselt number
p	Axial fin pitch (m)
P	Pressure (Pa)
$\tilde{p}$	Periodic pressure (Pa)
Pr	Prandtl number
q	Heat flux (W/m^2)
$\dot{Q}$	Heat transfer rate (W)
r	Radial distance from the center of the tube
$\vec{r}$	Position vector
R	Momentum transfer roughness function
R_o	Average radius of helically-finned tube
Ra	Rayleigh number
Re	Reynolds number
S	Momentum source term (N·s)
S_w	Swirl Number
St	Stanton number
t	Average rib width (m)
u	x-component of velocity vector
v	y-component of velocity vector
V	Velocity

V_m	Mesh volume
w	z-component of velocity vector
W	Weight

Greek Letters

α	Helix angle (°)
α' and α''	Corrugation shape angles (°)
β	Included angle (°)
Δ	Difference
Γ	Diffusion coefficient
μ	Dynamic viscosity (N·s/m^2)
ν	Kinematic viscosity (m^2/s)
ρ	Density (kg/m^3)
σ	Normal stress (Pa)
$\sigma_{k,\varepsilon}$	k-ε model constants
τ	Shear stress (Pa)

Subscripts

avg	Average
eff	Effective
eq	Equivalent
exp	Experimental
f	Fluid

fl	Fluent model
h	Hydraulic
i	Inside
in	Inlet
o	Annulus
p	Smooth tube
s	Solid
v.m.	Vortex mixing
z	Axial direction
θ	Tangential

CHAPTER 1
INTRODUCTION

1.1   <u>Background</u>

Currently, most of the electricity generated in the United States is

produced using coal, natural gas, or nuclear power. Published by the United

States Energy Information Administration, statistics show that coal, natural gas,

and nuclear power were used to produce more than 3,350 billion kilowatt-hours

or 89 percent of the net electricity generated in the United States during the year

2007. The Administration projects a 25% increase in the demand for electricity by

the year 2030 in the United States (EIA). Consequently, the supply of electricity

and the amount of fuel that is used to generate electricity must increase in order

to satisfy the projected demand. However, coal, natural gas, and nuclear power

are finite resources. As these resources become depleted, they become more

precious, and the efficient use of such fuels becomes increasingly important.

Moreover, mounting concerns about the adverse effects of green house gases,

which are byproducts of burning fossil fuels, and the current direction of

environmental legislation are pushing for lower emissions and greater efficiencies

with respect to generating electricity. There are many factors that affect the

efficient use of fuels with respect to generating electricity. One factor is the

process of converting a fuel into electricity. By improving this process or parts of

this process, a fuel can be used more efficiently, which can help increase the supply of electricity and meet the rising demand.

Most electricity is created using steam and steam turbines. A simple steam cycle diagram illustrates the basic process that is most commonly used to convert the potential energy of coal, natural gas, or nuclear power into electricity. Illustrated as a schematic in Figure 1.1, the basic Rankine cycle is an ideal model of the steam cycle that is commonly used by steam power plants to generate electricity. Note that the schematic illustrated in Figure 1.1 is only a basic model. Several other components of an actual cycle are omitted for simplicity. Hence, Figure 1.1 does not represent a complete steam cycle that is used to generate electricity. It is noted that the Rankine cycle is discussed exclusively in terms of water. No other fluids are considered in conjunction with the Rankine cycle.
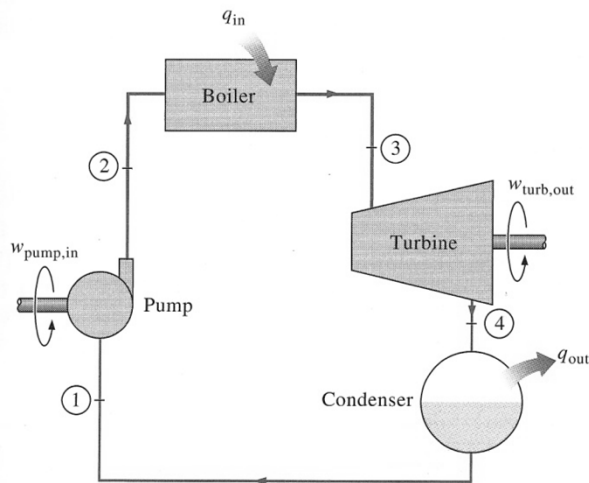
Figure 1.1.   The Rankine Cycle [Çengel (2006)].

As illustrated in Figure 1.1, the Rankine cycle consists of four key components and four basic processes. Although there are complex thermodynamic phenomena occurring at every stage of the cycle, a general

understanding of all of the processes and the purpose of each component is rudimentary.

The component of the Rankine cycle that is associated with the first process is the pump; this process occurs from Stage 1 to Stage 2. During this process, the function of the pump is twofold in that it compresses the saturated liquid water to the operating pressure of the boiler, and it transports the saturated liquid water to the boiler, where the second process of the Rankine cycle begins.

Positioned between Stages 2 and 3, the boiler functions as a large heat exchanger. Although the function of the boiler is simple, the intricate design of the boiler is a major focus of ongoing research, as the performance of the boiler significantly affects the overall efficiency of the cycle. The boiler is discussed in greater detail in the next section. The basic function of the boiler is to transfer heat from combustion gases, nuclear reactors, or other heat-energy sources to the saturated liquid water that is coming from the pump. As the water absorbs the heat, the phase of the water changes from a saturated liquid to a superheated vapor, and the third process of the Rankine cycle begins.

After the water becomes a superheated vapor, it passes from the boiler to the turbine, which is located between Stages 3 and 4. As the vapor enters into the turbine, it begins to cool, expands, and causes the turbine blades and turbine shaft to rotate. An electric generator is connected to the shaft. As the turbine shaft rotates, the shaft that is connected to the electric generator rotates simultaneously, and the electric generator produces electricity. Well designed electric generators and turbines are critical for producing electricity efficiently.

However, current research and design of the turbine and the electric generator are not presented, as such topics are beyond the scope of this research.

After the steam exits the turbine, it enters the condenser, which is the final component of the basic Rankine cycle and located between Stages 4 and 1. The purpose of the condenser is to reject large amounts of heat from the steam to a heat sink and condense the steam into a saturated liquid at constant temperature and pressure. Finally, the saturated liquid water is fed back into the pump, and the cycle repeats.

The Rankine cycle is an essential part of the technology that is used to generate electricity. However, the Rankine cycle is an ideal model, and it does not reflect the actual thermodynamic processes that occur in a real steam cycle. For example, the Rankine cycle does not account for the loss of energy due to fluid friction or the effects of irreversible processes. Nonetheless, the Rankine cycle is useful, and it provides insight into an ideal model of the steam cycle. Although a perfect steam cycle does not exist, it can be enhanced and optimized through innovation and strategic design of key components. One of the key components of the steam cycle is the boiler, which is discussed in the next section.

1.2   The Boiler and Helically-Finned Tubes

As briefly discussed earlier, the function of a boiler, or steam generator, is quite simple. A boiler transfers heat energy from a heat source to liquid water and induces a phase change as liquid water absorbs heat and becomes steam.

However, the intricate networks and designs of the components that comprise the modern boiler are not rudimentary.

Today, there are many types of boilers that are available on the market. Boilers may differ by various characteristics such as size, steam capacity, fuel source, convection technology, and other distinctions. In Figure 1.2, a schematic of a 750-megawatt once-through coal-fired utility boiler is illustrated and detailed with some of the major components that comprise the unit. The terms that are used to describe the boiler in Figure 1.2 are clarified in subsequent paragraphs of this section.
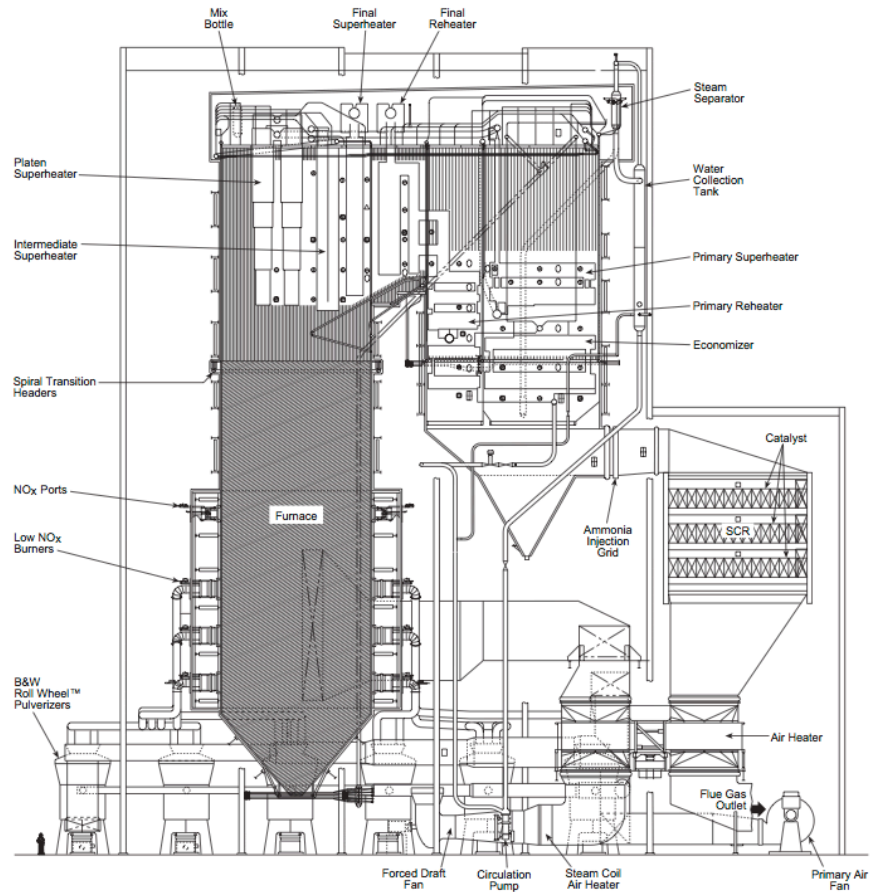
Figure 1.2   750 MW Once-Through Coal-Fired Utility Boiler [Stultz (2005)].

Although there are many individual components that make up the boiler, only the boiler tube is discussed, since it is the primary focus of this research. Note that the boiler tubes are not labeled in Figure 1.2. Nevertheless, they are located throughout the furnace area.

With respect to steam generators, a boiler tube is a pipe through which water flows and facilitates heat transfer from a heat source to the internally flowing water, which ultimately changes into steam. The most effective way to convert liquid water into high-pressure steam, Stultz (2006) suggests, is to heat tubes that have a relatively small diameter and contain a continuous flow of water. Using this method, there are two basic types of boiling systems that are used to generate high-pressure steam: a steam drum and a once-through steam generator (OTSG). Both systems are illustrated in Figure 1.3.
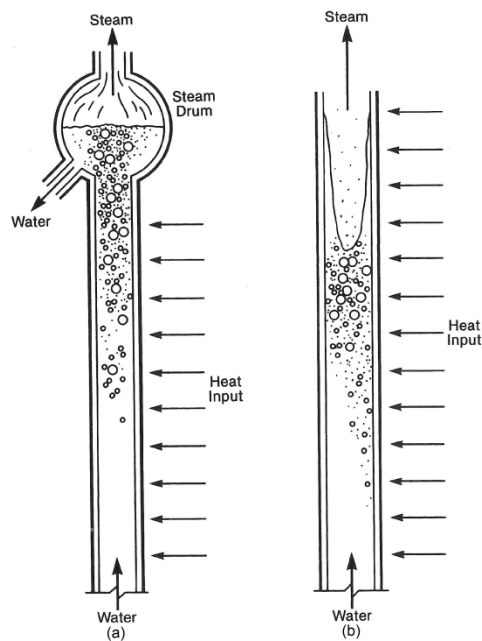
Figure 1.3   Boiling Systems [Stultz (2005)]. (a) Steam Drum, (b) Once-Through Steam Generator (OTSG)

6

In a steam drum boiling system, water is heated to its boiling point inside the tube and changes into a steam-water mixture as it approaches the steam drum. As the steam-water mixture enters the steam drum, the steam and the water begin to separate. The liquid portion of the mixture is recycled back into the heated tube, and the steam is directed out of the boiler system. With the exception of the drum portion of the steam drum system, the once-through steam generator operates in a similar fashion.

In a once-through boiling system, subcooled water is heated as it travels through the tube. The amount of heat that is directed toward the flowing water is carefully controlled such that the water flowing through the tube fully changes into steam before exiting the system. Since all of the water in the system is converted into steam, there is no need for a steam drum. However, there are several important factors to consider in order to ensure that all of the subcooled water is converted into steam in a once-through boiling system. Such factors are: pipe length, heat input, water flow rate, rate of heat transfer, and the pressure drop along the pipe. Arguably, this list is incomplete. Nevertheless, the rate of heat transfer and the pressure drop along the pipe are two of the most studied characteristics with respect to the boiler tube.

According to Newton's Law of Cooling, the rate of convection heat transfer between a solid and a fluid is proportional to the temperature difference between the solid and the fluid by a factor of the product of the surface area through which convective heat transfer takes place and the convective heat transfer coefficient. Mathematically, Newton's Law of Cooling states

$$\dot{Q} = hA_s(T_s - T_f) \qquad (1)$$

In conjunction with Equation (1), consider the boiler tubes that are illustrated in Figure 1.4 – the thickness and the diameter of both tubes are equal. Suppose that an identical fluid with the same temperature is moderately flowing through each tube, and the wall temperature of each tube is the same, but the wall temperatures differ from the temperature of the fluid. Equation (1) asserts that the rate of heat transfer occurring in Tube (b) is greater than the rate of heat transfer occurring in Tube (a). This is true for several reasons. The most apparent reason is that the area through which convective heat transfer takes place in Tube (b) is greater than the area in Tube (a), as a result of the presence of transverse fins in Tube (b). Furthermore, the conductive heat transfer coefficient associated with Tube (b) is higher than the coefficient associated with Tube (a) as a result of greater turbulence and better mixing within Tube (b).

(a)   (b)
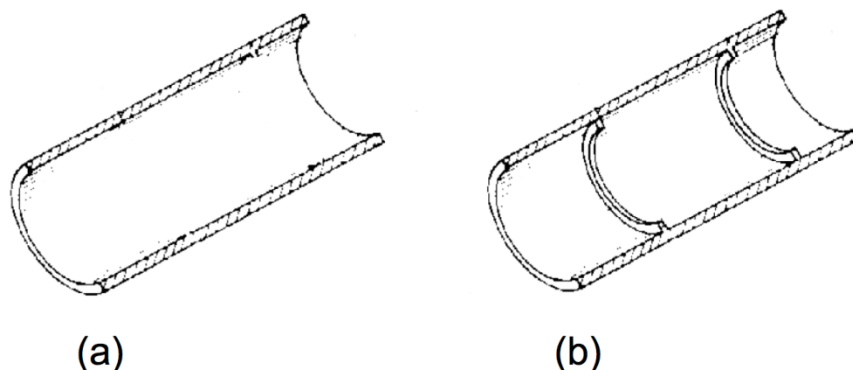
Figure 1.4   Tube Surface. (a) Smooth Tube, (b) Tube with Transverse Fins.

The presence of fins in Tube (b) is called an enhancement. As the change

in the surface geometry increases, compared to Tube (a), the rate of heat

transfer increases, too. There are many kinds of tube enhancements, such as rib

configurations, roughened surfaces, and corrugations. Some of the most

common tube enhancements are presented by Webb (1982). Several

configurations are illustrated in Figure 1.5.
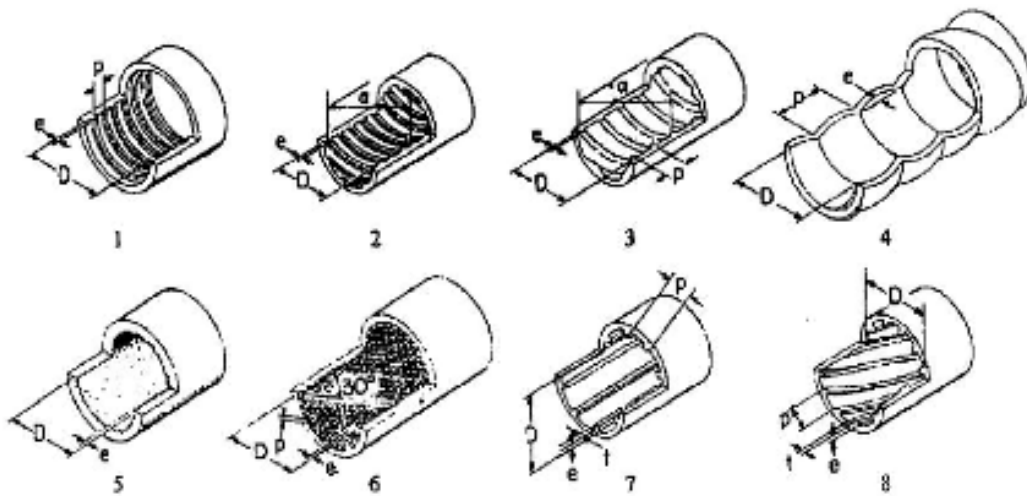
Figure 1.5   Enhanced Tube Configurations [Webb (1982)]. 1. Transverse
             Rib, 2. Helical Rib, 3. Turbo-Chil Rib, 4. Corrugated, 5. Sand-
             Grain, 6. Three-Dimensional, 7. Axial-Fin, 8. Helical Fin.

In addition to increasing the rate of heat transfer, tube enhancements also

increase the pressure drop along the pipe as a result of an increase in surface

area, an increase in turbulence, and boundary layer disruptions. Being able to

predict and knowing the pressure drop that occurs along an enhanced tube is

often key. The design of steam generators is one particular area of research

where enhanced tubes are used to increase the rate of heat transfer. Knowing the pressure drop along such tubes is important for good design.

One common tube configuration that is often used in once-through steam generators is the helical fin. An example of a helically-finned tube is illustrated in Figure 1.5, Enhanced Tube Configuration number 2. There are six geometric parameters that define the configuration of the helically-finned tube. Each parameter is defined pictorially in Figure 1.6. The fin pitch, (p), is the axial distance along the pipe between the centers of two consecutive fins. The fin height, (e), is the distance between the inner diameter of the tube and the top of the fin. The helix angle, (α), is the angle that is formed between the fin and the axis of the tube. The included angle, (β), is the angle at which the sides of the fin meet. The diameter, (D), is the maximum internal diameter of the pipe, and the fin width, (t), is the distance between the two sides of the fin, measured at the vertical center of the fin.
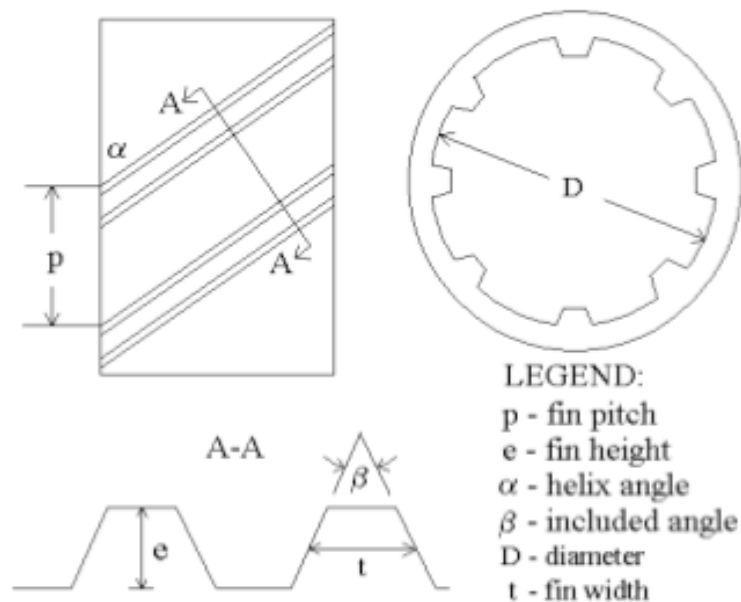
Figure 1.6   Geometric Variables of the Helical Fin [Zdaniuk (2006)].

Currently, no closed formula exists for predicting the pressure drop along a helically-finned tube. Only empirical correlations are available. Over the past few decades, several scientists have studied the complex flows that occur in helically-finned tubes and have tried to develop techniques for modeling the pressure drop in a concise fashion. Although progress has been made, no one has been completely successful. The primary reason for this is lack of experimental data. The purpose of this thesis is to develop and verify numerical simulation techniques that can be used to model a pressure drop along a helically-finned tube. This technique could be used to generate more data, form better correlations, and fashion a closed formula that accurately predicts the pressure drop along a helically-finned tube.

1.3   Literature Review

The purpose of this section is to document several of the articles that were reviewed during the creation of this thesis. Although the primary topic of this thesis is pressure drop along helically-finned tubes, some of the information that is presented concerns heat transfer as well. Typically, scientists who study helically-finned tubes consider the effects of both pressure drop and heat transfer.

Li et al. (1982) conducted several experiments to better understand pressure drop and heat transfer properties of helically-finned tubes. Initially, Li et al. (1982) conducted qualitative flow visualization experiments where hydrogen bubbles were injected into a flow stream of water inside a helically-finned tube.

The paths of the hydrogen bubbles were captured using a high-speed camera, and the photographs were analyzed in order to qualify the visual properties of the flow. During this experiment, the researchers considered four different tube samples with various geometric parameters. Of the samples, the number of starts was one or three, and the helix angles ranged from 38º to 80º.

Li et al. (1982) examined laminar and turbulent flow regimes for each of the tube samples. With respect to a laminar flow, it was reported that the hydrogen bubbles created parabolic patterns along the pipe. However, the parabolic paths did not exist in the turbulent flows due to the presence of flow separation. The research team also reported that the hydrogen bubbles inside the tubes with smaller helix angles did not follow the trend of the fins as closely as the bubbles inside the tubes with larger helix angles.

Li et al. (1982) also performed additional experiments in order to quantify the performance of a helically-finned tube. This study considered 20 helically-finned brass tubes. The helix angles ranged from 41.4º to 81.8º, and the number of starts ranged from one to four.

In order to quantify the performance of the tubes, Li et al. (1982) reported the results of the experiments in terms of a roughness factor of momentum transfer, *R,* and heat transfer, *G.* For single start tubes, the following correlations were reported:

$$R = 0.995\left(\frac{e}{D}\right)^{-0.156}\left(\frac{p}{e}\right)^{0.465}\left(\frac{\alpha}{90}\right)^{0.484}\exp\left(\frac{(\ln(\text{Re})-9.62)^2}{1000(p/e)^{-1.38}}\right) \tag{2}$$

$$G = 0.478 \left(\frac{e}{D}\right)^{-0.1621} \left(\frac{\alpha}{90}\right)^{-0.869} (e+)^{0.641+0.105\ln(e/D)} \Pr^{0.57} \tag{3}$$

where the roughness Reynolds number, e+, was defined to be

$$e+ = \frac{e}{D}\text{Re}\sqrt{\frac{f}{2}} = \frac{eu^*}{v} \tag{4}$$

Furthermore, Li et al. (1982) reported that the following equation represented the roughness function of momentum transfer for all of the tubes that were studied; *i.e.* tubes with one to four starts.

$$R = \sqrt{\frac{2}{f}} + 2.5\ln\left(\frac{2e}{D}\right) + 3.75 \tag{5}$$

Combining Equations (2) and (5), Li et al. (1982) was able to develop the following correlation between the Fanning friction factor, the Reynolds number, and the geometric parameters of a helically-finned tube:

$$\sqrt{\frac{f}{2}} = 3.42\ln\left(\frac{D}{2e}\right) - 4.64 + 1.25\left(\frac{e}{D}\right)^{-0.057}\left(\frac{p}{e}\right)^{0.5}\left(\frac{\alpha}{90}\right)^{1.14}\exp\left(\frac{(\ln(\text{Re})-9.62)^2}{1000(p/e)^{-1.38}}\right) \tag{6}$$

However, they developed the correlation using the data from the single start tubes, only. Thus, the correlation is only applicable for tubes with a single start, or $N_s = 1$.

Belyakov et al. (1989) conducted a study and examined the hydraulic resistance, or pressure drop, of 13 helically-finned tubes. The tube samples

13

varied in terms of fin geometries, tube sizes, and fin types. The various fin types

that were considered in the study are illustrated in Figure 1.7. Developing a

model for the hydraulic resistance of the tubes, the researchers divided the

vector of the mean flow velocity into two components. One component was the

velocity vector that was parallel to the direction along the helical fins, and the

other component was the velocity vector that was perpendicular to the parallel

component. The principle of superposition was used to determine the effects of

the hydraulic losses due to friction, the swirling of the flow (or vortex mixing), and

flow separation about the fins. During this study, a correlation for each of the

hydraulic losses was developed.
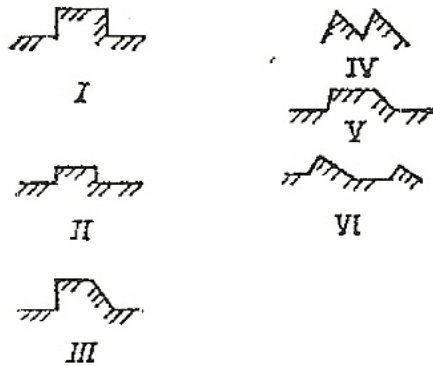
Figure 1.7   Fin Types Considered by Belyakov et al. (1989).

For the frictional resistance factor, Belyakov et al. (1989) proposed the

following equation:

$$\Delta P_{friction} = 2f_{friction}\rho V^2_{parallel} \frac{L_{equivalent}}{D_h} = 2f\rho V^2 \frac{L}{D_h} \tag{7}$$

While developing a correlation for the losses associated with the swirling flow, Belyakov et al. (1989) suggested that the liquid near the main boundary layer, which possesses a low velocity, enters the core of the flow and induces some retardation. Accounting for this effect in the momentum equation and carrying out calculations using the 1/7th power-law velocity profile, the researchers proposed the following equation in order to account for the hydraulic losses due to swirling flow.

$$4f_{v.m.} = \frac{0.180}{Re} \frac{D}{pN_s} \left[1125 \ln \left(\frac{Re\sqrt{4f_p + 4f_{v.m.}}}{2} - 3170 \right) \right] \tag{8}$$

Hence, Belyakov et al. (1989) defined the overall resistance factor as:

$$f = f_{friction} + f_{v.m.} \tag{9}$$

Belyakov et al. (1989) suggested that the vortex losses associated with the perpendicular velocity component be incorporated. Hence, they developed the following equation to account for such losses:

$$\Delta P_{seperation} = 2f_{seperation}\rho V_{perpendicular}^2 \frac{L}{D} = 2f_{seperation}\rho V^2 \sin^2(\alpha)\frac{L}{D} \tag{10}$$

However, Belyakov et al. (1989) stated that "at present, [$f_{seperation}$] can be found only experimentally. It depends on form of the fins and their number." As a result, Belyakov et al. (1989) proposed the following overall resistance factor:

$$f_{overall} = \left(f_{friction} + f_{v.m.} \right) \cos^{3/4}(\alpha) + f_{seperation} \sin^2(\alpha)$$

$$= \left(\frac{0.316}{\sqrt[4]{\mathrm{Re}}} + f_{v.m.} \right) \cos^{3/4}(\alpha) + f_{seperation} \sin^2(\alpha)$$

(11)

During the experiment, Belyakov et al. (1989) correlated the overall resistance factor for the cases with Type I fins (reference Figure 1.7). Belyakov et al. (1989) proposed that the overall resistance coefficient for such tubes was:

$$4f = 0.115 \frac{\left(\sqrt[3]{\left(\frac{D-2e}{p\sin(\alpha)} \right)^2} \log\left(\frac{p\sin(\alpha)-t}{e} \right) \right)^2}{\left(\log\frac{D}{e} \right)^2}$$

(12)

An experiment that was conducted by Webb et al. (2000) considered seven helically-finned tubes with 18 to 45 starts, helix angles between 25⁰ and 45⁰, rib heights between 0.33 mm and 0.55 mm, and a constant $D_i = 15.54$ mm. In this study, Webb et al. (2000) developed two correlations that related the friction factor to geometric variables and Reynolds numbers. One correlation was developed using linear multiple regression, and the other correlation was developed using the heat-momentum transfer analogy for rough surfaces, which was developed by Webb et al. (2000). The researchers reported that the average deviation of the correlation based on the heat-momentum transfer analogy for rough surfaces was higher than the average deviation of the multiple regression correlation for predicting the friction factor of the enhanced tubes.

With respect to the linear multiple regression correlation, Webb et al. (2000) reported the following equation:

$$f = 0.108 \mathrm{Re}^{-0.283} N_s^{0.221} \left(e/D_i\right)^{0.785} \alpha^{0.78} \tag{13}$$

Lastly, the researchers obtained the following correlation using the momentum transfer analogy for rough surfaces:

$$\sqrt{2/f} = 4.762(e+)^{0.2138} N_s^{-0.1096} \alpha^{-0.297} - 2.5\ln(2e/D_i) - 3.75 \tag{14}$$

An experiment performed by Jensen and Vlakancic (1999) examined the hydraulic performance of 15 helically-finned tubes with the number of starts ranging from 8 to 54, the helix angles ranging from 0° to 45°, the fin-widths ranging from 0.62 mm to 1.84 mm, and the ratios of e/D ranging from 0.62 to 1.84. During this study, Jensen and Vlakancic (1999) identified two types of flows that occurred in the finned tubes. The first type was described as fluid flow that tended to follow the spaces in between the helical fins as the fluid traveled along the tube. Jensen and Vlakancic (1999) referred to this type of flow as swirl flow. Moreover, they reported that the first type of flow occurred in tubes with relatively small helix angles ($\alpha \leq 30^\circ$), large fins heights, and few starts. The second type of flow was described as an occurrence where the inter-fin regions exhibited enough resistance to the flow that the main portion of the flow was constrained to the center region of the tube and skipped over the fins. As a result, the inter-fin regions were susceptible to relaminareization. Having recognized the two types of flows, Jensen and Vlakancic (1999) developed a separate correlation for each

type. Thus, the appropriate correlation for each tube was dependent upon the type of flow that the helically-finned tube induced.

The friction factor correlation that Jensen and Vlakancic (1999) developed for the first type of flow was given as:

$$\frac{f}{f_p} = \left(\frac{l_{csw}}{D}\right)^{-1.25}\left(\frac{\pi\frac{D^2}{4}}{\pi\frac{D^2}{4} - N_s et}\right) \tag{15}$$

where

$$\frac{l_{csw}}{D} = \frac{l_c}{D}\left[1 - 0.203p_{modified}^{0.65}(2e/D)^{0.20}\right] \tag{16}$$

and,

$$\tag{17}$$

$$\frac{l_c}{D} = \frac{\pi\frac{D^2}{4}(1 - 2e/D)^2}{\pi\frac{D^2}{4} - N_s et}(1 - 2e/D) + \left[1 - \frac{\pi\frac{D^2}{4}(1 - 2e/D)^2}{\pi\frac{D^2}{4} - N_s et}\right]\left[\frac{\pi}{N_s}(1 - 2e/D) - \frac{t}{D}\right]$$

In conjunction with Equation (15), Jensen and Vlakancic (1999) proposed the following correlations for helically-finned tubes that induced the second type of flow:

$$\frac{l_{csw}}{D} = \left[1 - 1.577p_{modified}^{0.64}(2e/D)^{0.53}\left[(\pi/N_s - t/D)\cos(\alpha)\right]^{0.28}\right] \quad \text{for} \quad e/D \le 0.02$$
$$\text{Re} \ge 20,000 \tag{18}$$

$$\frac{l_{csw}}{D} = \left[1 - 0.994p_{modified}^{0.89}(2e/D)^{0.44}\left[(\pi/N_s - t/D)\cos(\alpha)\right]^{0.41}\right] \quad \text{for} \quad 0.02 \le e/D \le 0.03$$
$$\text{Re} \ge 20,000 \tag{19}$$

18

Zdaniuk et al. (2008) conducted a study where the friction factors were experimentally determined for eight helically-finned tubes at Reynolds numbers ranging between 12,000 and 60,000. The tubes that were studied in the experiment had helix angles between 25º and 48º, fin height-to-diameter ratios between 0.0199 and 0.0327, and number of starts between 10 and 45. Zdaniuk et al. (2008) developed a power-law correlation for the Fanning friction factor using a least squares regression approach that was based on the experimental measurements of the friction factors of the eight helically-finned tubes. The researchers also investigated the relationship between varying the geometric parameters and the friction factor.

Zdaniuk et al. (2008) obtained the following correlation for the Fanning friction factor of the eight helically-finned tubes:

$$f = 0.128 \mathrm{Re}^{-0.305} N_s^{0.235} (e/D)^{0.319} \alpha^{0.397}$$
(20)

With respect to the influence of the geometric parameters on the friction factor results, the researchers reported that the Fanning friction factor increased with increasing number of starts, helix angles, and fin height-to-diameter ratios, for the most part. They reported that one exception did occur where Tube A and Tube B had fin height-to-diameter ratios of 0.0243 and 0.0244, respectively, and the Fanning friction factor that was measured in Tube B was higher than the Fanning friction factor that was measured in Tube A. Zdaniuk et al. (2008) attributed this discrepancy to the high helix angles of both tubes and suggested that the results were a consequence of the development of a skimming flow.

1.4   Scope of Work

The primary goal of this thesis is to numerically model a fluid flow within a

helically-finned tube and determine the fluid friction factor associated with the

tube geometry and Reynolds number using a computational fluid dynamics

(CFD) software and three distinct modeling techniques. In order to create an

acceptable model, experimental data for a helically-finned tube of known

geometric parameters and Reynolds numbers was obtained from an experiment

that was performed at Mississippi State University and published by Zdaniuk et

al. (2008). Zdaniuk et al. (2008) examined eight helically-finned tubes with

various geometric parameters at various Reynolds numbers. However, only one

tube configuration at seven Reynolds numbers was considered in this thesis. The

tube that was chosen for simulation had the following geometric properties: helix

angle of 25º, 10 starts, fin height of 0.38 mm, internal nominal diameter of 15.64

mm, and fin pitch of 10.54 mm. The fin width was 0.48 mm at the fin base, and

0.2 mm at the fin tip. The Reynolds numbers that were considered ranged

between 12,000 and 56,000. After the helically-finned tube to be examined was

chosen, along with the Reynolds numbers, three-dimensional models of the

internal fluid within the pipe were created.

Models of the fluid were constructed using the mechanical computer aided

design (CAD) software SolidWorks. Two distinct types of SolidWorks models of

the fluid were created. However, the key geometric parameters of both models

were equivalent. The first type of model is used in conjunction with the first and

second modeling techniques, and the second type is used in conjunction with the

third modeling technique. After the models were created with SolidWorks, they were imported into a preprocessor program.

Fluent Gambit was the preprocessor software that was used to edit the geometries that were imported from SolidWorks and mesh the models of the fluid. Each of the two models was imported into Gambit and meshed separately. The model associated with the first modeling technique was meshed using a relatively coarse mesh. A coarse mesh was used because of the extensive length of the model, and because the computing time required to solve the model with a fine mesh was not justifiable. The models associated with the second and third modeling techniques were meshed using a relatively fine mesh. Fine mesh elements were used because of the relatively short length of the models. After the meshed models were created, they were imported into a CFD software for simulation.

Fluent, by Ansys, Inc., was the CFD software that was used to simulate the fluid flow within the helically-finned tube and determine the friction factor. With respect to the first modeling technique, the corresponding mesh was imported into Fluent, and the appropriate boundary conditions were applied to the mesh. In the first simulation, the velocity associated with the least Reynolds number was programmed into the model. The model was solved on a cluster using parallel processors. A journal file was created and used with Fluent in order to carry out text user interface commands in Fluent on the cluster. Lastly, the simulation was submitted to the cluster, and the simulation was solved. This

process was repeated for each of the seven Reynolds numbers that was associated with the data published by Zdaniuk et al. (2008).

A second modeling technique was employed in order to solve the same simulation that was previously described. The mesh associated with the second modeling technique was imported into Fluent, and the appropriate boundary conditions were programmed into the model. Again, this model was solved on a cluster, and a journal file was required. However, this particular modeling technique required a two-part journal file. The first part of the journal file was similar to that which was used in the first technique. The second part contained a series of repetitive commands. The journal file was created, and the simulation was submitted to the cluster and solved. This process was repeated for each of the seven Reynolds numbers.

Lastly, a third modeling technique was employed in order to solve the simulation for each of the seven Reynolds numbers previously mentioned. The mesh associated with this technique was imported into Fluent, and the appropriate boundary conditions were programmed into the model. A journal file, similar to the one used in the first technique, was created, and the simulation was submitted to the cluster and solved. Again, the process was repeated for each of the seven Reynolds numbers.

After the simulations for each of the seven different Reynolds numbers were solved, using the three distinct modeling techniques, each of the 21 solution files were examined using a postprocessor program, and the solution data was analyzed. The friction factor associated with each of the helically-finned tubes

was calculated using the data from each simulation. Finally, the experimentally determined friction factors were juxtaposed with the numerical friction factors. The results were documented.

CHAPTER 2
EXPERIMENTAL DATA

2.1   <u>Experimental Tubes</u>

The experimental data presented and used for comparison in this thesis was obtained from a laboratory experiment performed at Mississippi State University. The experiment was devised to measure the turbulent pressure drop and heat transfer performance in helically-finned tubes. The complete laboratory experiment and corresponding results were published by Zdaniuk et al. (2008). Experimental data for this thesis was not obtained directly by the author or Youngstown State University because replicating a similar experiment was neither financially possible nor practical. Nevertheless, the objective of this thesis was fulfilled.

The purpose of this chapter is to describe the experimental setup and the process that was used to collect the friction factor portion of the data, as described by Zdaniuk et al. (2008). The experiment examined eight helically-finned tubes and one plain tube. These tubes were manufactured by Wieland-Werke AG of Ulm, Germany. Each tube was 10 feet long and made of copper-nickel. However, only 9 feet of the surface of the helically-finned tubes were finned. The remaining 1 foot section of each helically-finned tube was plain for installation purposes. The primary geometric parameters of each of the nine tubes are shown in Table 2.1. The axial bases of the fins measured 0.48 mm,

24

and the included angle, β, of fins measured 41°. It is noted that roughness-height

of the internal surfaces of the helically-finned tubes was not provided by Zdaniuk

et al. (2008) (or the manufacturer). See Figure 1.6 in Chapter 1 for an illustrative

reference to the tube geometries.

Table 2.1   Tube Geometries by Zdaniuk et al. (2008)

Tube Identification	Number of Starts	Fin Height	Helix Angle	Internal Nominal Diameter
-	N_s	e	α	D
(-)	(-)	(mm)	(°)	(mm)
1	10	0.380	25	15.64
2	30	0.375	25	15.61
3	30	0.380	48	15.62
4	45	0.380	25	15.57
5	45	0.310	35	15.6
6	45	0.380	35	15.57
7	45	0.510	35	15.59

2.2   Experimental Setup

A schematic of the experimental setup that was used by Zdaniuk et al.

(2008) to collect the experimental data is shown in Figure 2.8. The schematic

illustrates a double-pipe counterflow heat exchanger. Although the thermal

properties of the helically-finned tubes are beyond the scope of this thesis, an

inclusive description of the experimental setup, as described by Zdaniuk et al.

(2008), is presented for the purpose of completeness.

The experimental apparatus consisted of a hot water loop, a cold water

supply, and several other components. The hot water loop included a storage

tank, a 15 kW heating element, a 1-hp pump, a test tube, and two ball valves that

were used to control the velocity of the water. The cold water was supplied by the

city and entered the apparatus at approximately 20°C. There were two ball

valves available in order to control the velocity of the cold water. Zdaniuk et al.

(2008) reported that all of the tubes of the apparatus were insulated.
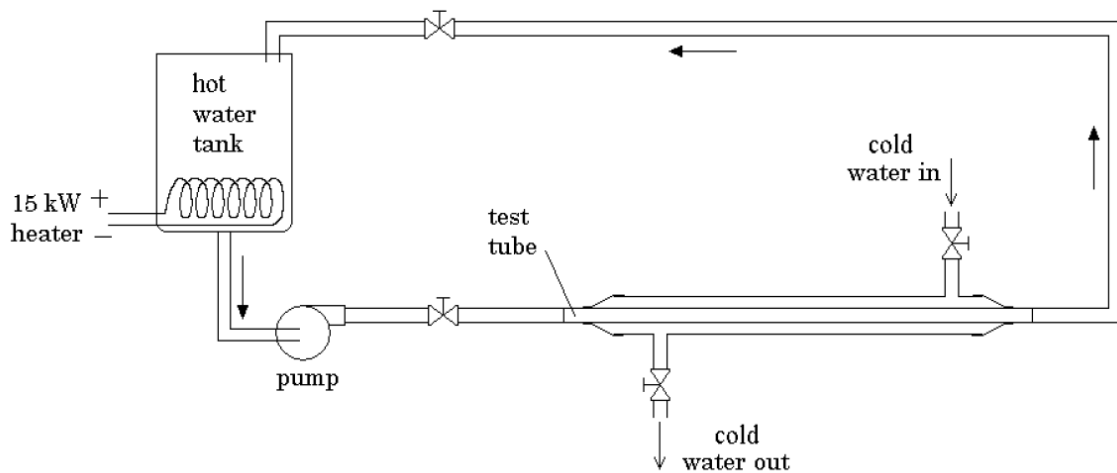
Figure 2.1.   Schematic of Experimental Apparatus. [Zdaniuk et al. (2008)]

A detailed schematic of the test section was provided by Zdaniuk et al.

(2008) and is illustrated in Figure 9. To measure the pressure drop along the test

tubes, two pressure taps were installed before and after the test section.

Sensotec differential pressure transducers (model TJE) were used to measure

the pressure at each of the pressure taps. The manufacturer of the transducers

reported an accuracy of 0.1%. In order to measure the inlet and exit

temperatures of the hot and cold water, thermocouples were installed inside of

the tees. The flow rate of the water inside the test tube was measured using an

Omega FP-53000 flow meter, which had an accuracy of 0.2 ft/s. Similarly, the

flow rate of the cold water was measured using a Hersey 1006 flow meter, which

had an accuracy of 1.0%
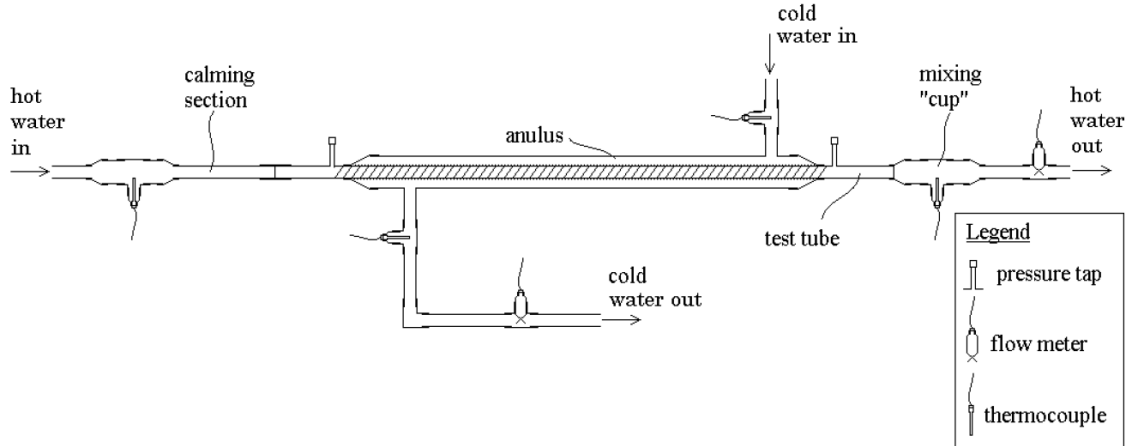
Figure 2.2.   Detailed Schematic of Test Section [Zdaniuk et al. (2008)].

After the transducers, thermocouples, and flow meters were installed and

calibrated, each of the measuring devices was connected to an SCXI data

acquisition system from National Instruments. An interface program was created

using LabVIEW 6.1 in order to facilitate hardware control and data collection. The

reader is directed to Zdaniuk et al. (2008) for more detailed information regarding

the setup of the experiment.

After the pressure drop data for each of test tubes was collected, the

Fanning friction factor was calculated using the following formula:

$$f = \frac{\Delta P D}{L \rho V^2}$$

(21)

where ΔP is the pressure drop between the pressure taps, D is the nominal

inside diameter of the test tube, L is the distance between the pressure taps, ρ is

the density at the mean bulk temperature, and *V* is the average velocity based on the nominal diameter.

After completing the experiment, Zdaniuk et al. (2008) reported the following friction factor results for the various tube configurations at various Reynolds numbers:
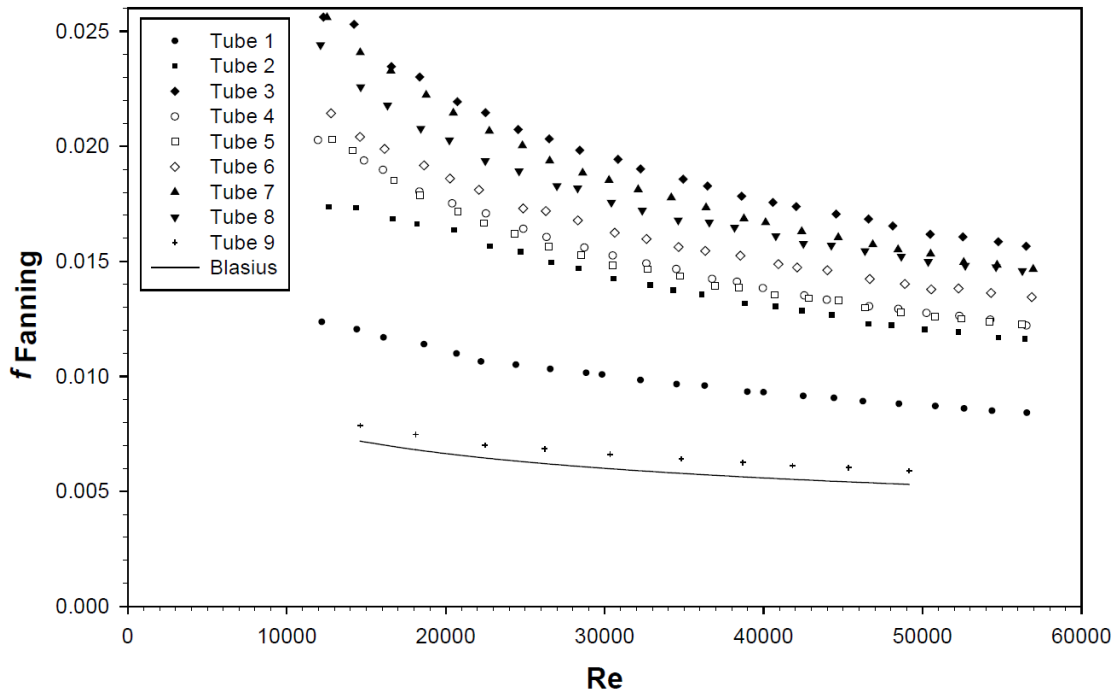
Figure 2.3.   Experimental Results of Zdaniuk et al. (2008)

Tube 1 was the tube configuration that was considered for this thesis. However, only seven of the corresponding Reynolds numbers were considered. The tube configuration and the Reynolds numbers that were considered are discussed in greater detail in later chapters.

CHAPTER 3

MATHEMATICAL MODEL OF FLUID FLOW

In order to study the fluid flow within a helically-finned tube, a mathematical model(s) is needed. The model that is used in a computational fluid dynamics (CFD) program is a set of governing equations that describe the physical phenomena within the fluid domain. Fluent was the CFD software that was used to simulate the turbulent fluid flow within a helically-finned tube, as part of this thesis. The purpose of this section is to introduce the basic governing equations that are used by Fluent to simulate fluid flow.

3.1   Mathematical Model

The primary fundamental equations that are used to model the fluid flow within a helically-finned tube are the continuity equation, momentum equation, and energy equation. These equations are derived from physical laws of nature. However, these equations do not fully model the fluid flow as a result of the inherent complexities of turbulent flow, which were expected to occur within the finned tube. Therefore, the transport equations for the standard k-ε model for the turbulent kinetic energy and the rate of its dissipation are considered.

In deriving the governing equations of the fluid motion within a helically-finned tube, the following assumptions were made:

1. The fluid is Newtonian

2. The fluid is incompressible.

3. Body forces are negligible.

4. There is no viscous dissipation.

5. The flow within the tube is turbulent.

3.1.1 Continuity Equation

The law of conservation for fluid flow asserts that the mass within a control volume of fluid is always conserved. Hence, the continuity equation, in terms of fluid dynamics, is sometimes referred to as the conservation of mass equation. Since the mass of the control volume is conserved, the net quantity of matter within the control volume is constant at all times. This statement can be expressed mathematically by the following equation:

$$\frac{\partial \rho}{\partial t} + \nabla \cdot \rho \vec{V} = 0 \qquad\qquad (22)$$

where

$\dfrac{\partial \rho}{\partial t}$ $\equiv$ rate of change of the density inside the control volume

∇ $\equiv$ vector differential operator in Cartesian coordinates

$\nabla \cdot \rho \vec{V}$ $\equiv$ net mass flow accross boundaries of the control volume

3.1.2 Momentum Equation

The law of conservation of momentum is a direct result of Newton's second law of motion, which states that the net force on a particle, or an object,

30

is equal to the time rate of change of its linear momentum. Applying this law to a fluid element in three-dimensional space, three momentum equations are formed, one equation for each of the three spatial coordinates. Hence, for the x-coordinate, the law asserts that the rate of change of momentum in the x-direction of the fluid element is equal to the total force on the element in the x-direction and the rate of increase of the momentum in the x-direction due to sources. The law is applied to the remaining two spatial coordinates in a similar fashion. Expanding the surface forces and keeping the body forces as a single term, the mathematical form of the law of conservation of momentum for each of the three coordinates is given by the following set of differential equations:

$$\frac{\partial(\rho u)}{\partial t} + \nabla \cdot \rho \vec{V} u = dF_{Bx} + \frac{\partial \sigma_{xx}}{\partial x} + \frac{\partial \tau_{yx}}{\partial y} + \frac{\partial \tau_{zx}}{\partial z} + S_{Mx} \qquad (23a)$$

$$\frac{\partial(\rho v)}{\partial t} + \nabla \cdot \rho \vec{V} v = dF_{By} + \frac{\partial \tau_{xy}}{\partial x} + \frac{\partial \sigma_{yy}}{\partial y} + \frac{\partial \tau_{zy}}{\partial z} + S_{My} \qquad (23b)$$

$$\frac{\partial(\rho w)}{\partial t} + \nabla \cdot \rho \vec{V} w = dF_{Bz} + \frac{\partial \tau_{xz}}{\partial x} + \frac{\partial \tau_{yz}}{\partial y} + \frac{\partial \sigma_{zz}}{\partial z} + S_{Mz} \qquad (23c)$$

where

$\vec{V}$ $\equiv$ total velocity vector of the fluid

u, v, w $\equiv$ $x, y,$ and z components of the velocity, respectively

σ_{ii}, τ_{ij} $\equiv$ normal and shear viscous stress terms, respectively

dF_{Bi} $\equiv$ differential body force component

S_{Mi} $\equiv$ momentum source term component

3.1.3 <u>Navier-Stokes Equations</u>

The relationship between the viscous stress and the shear strain of a fluid is an important physical property of a fluid and is used extensively in the study of fluid dynamics. The fluid that is considered in this thesis is water, which is an isotropic Newtonian fluid. Hence, the viscous stress at any point within the fluid domain is directly proportional to the rate of shearing strain, or rate of angular deformation, at that point. In a three dimensional setting, there are nine viscous stress components to consider. Of the nine stress components, there are three normal stress components and six shear stress components. However, only three of the six shear components are independent. In Cartesian coordinates, the nine stresses may be expressed mathematically in terms of velocity gradients and fluid properties as follows:

$$\tau_{xy} = \tau_{yx} = \mu \left(\frac{\partial v}{\partial x} + \frac{\partial u}{\partial y} \right) \tag{24a}$$

$$\tau_{yz} = \tau_{zy} = \mu \left(\frac{\partial w}{\partial y} + \frac{\partial v}{\partial z} \right) \tag{24b}$$

$$\tau_{zx} = \tau_{xz} = \mu \left(\frac{\partial u}{\partial z} + \frac{\partial w}{\partial x} \right) \tag{24c}$$

$$\sigma_{xx} = -p - \frac{2}{3} \mu \nabla \cdot \vec{V} + 2\mu \frac{\partial u}{\partial x} \tag{24d}$$

$$\sigma_{yy} = -p - \frac{2}{3} \mu \nabla \cdot \vec{V} + 2\mu \frac{\partial v}{\partial y} \tag{24e}$$

$$\sigma_{zz} = -p - \frac{2}{3} \mu \nabla \cdot \vec{V} + 2\mu \frac{\partial w}{\partial z} \tag{24f}$$

where

$\mu \quad \equiv \quad$ fluid dynamic viscosity

$p \quad \equiv \quad$ local thermodynamic pressure

By substituting the six stress equations into the three momentum equations, the Navier-Stokes equations are formed. Upon substitution and rearrangement of several of the terms, the Navier-stokes equations may be expressed as follows:

$$\frac{\partial(\rho u)}{\partial t} + \nabla \cdot \rho \vec{V} u = -\frac{\partial p}{\partial x} + \nabla \cdot (\mu \nabla u) + S_{Mx} \tag{25}$$

$$\frac{\partial(\rho v)}{\partial t} + \nabla \cdot \rho \vec{V} v = -\frac{\partial p}{\partial y} + \nabla \cdot (\mu \nabla v) + S_{My} \tag{26}$$

$$\frac{\partial(\rho w)}{\partial t} + \nabla \cdot \rho \vec{V} w = -\frac{\partial p}{\partial z} + \nabla \cdot (\mu \nabla w) + S_{Mz} \tag{27}$$

By further expansion of each of the terms in each of the equations and implementation of the assumptions of the flow within a helically-finned tube, the Navier-Stokes equations are expressed in one of the most commonly known forms of the equations as follows:

$$\rho \left(\frac{\partial u}{\partial t} + u\frac{\partial u}{dx} + v\frac{\partial u}{\partial y} + w\frac{\partial u}{dz} \right) = -\frac{\partial p}{\partial x} + \mu \left(\frac{\partial^2 u}{dx^2} + \frac{\partial^2 u}{\partial y^2} + \frac{\partial^2 u}{dz^2} \right) \tag{28a}$$

$$\rho \left(\frac{\partial v}{\partial t} + u\frac{\partial v}{dx} + v\frac{\partial v}{\partial y} + w\frac{\partial v}{dz} \right) = -\frac{\partial p}{\partial y} + \mu \left(\frac{\partial^2 v}{dx^2} + \frac{\partial^2 v}{\partial y^2} + \frac{\partial^2 v}{dz^2} \right) \tag{28b}$$

$$\rho \left(\frac{\partial w}{\partial t} + u\frac{\partial w}{dx} + v\frac{\partial w}{\partial y} + w\frac{\partial w}{dz} \right) = -\frac{\partial p}{\partial z} + \mu \left(\frac{\partial^2 w}{dx^2} + \frac{\partial^2 w}{\partial y^2} + \frac{\partial^2 w}{dz^2} \right) \tag{28c}$$

3.1.4 <u>Transport Equation</u>

Turbulent flows are characterized by chaotic and rapid fluctuations in flow field properties. Some of the properties that are highly affected by a turbulent flow regime include pressure, velocity, low momentum diffusion, high momentum convection, and energy. These properties, or quantities thereof, are sometimes referred to as transported quantities. As each of these properties is intimately related to one another, small fluctuations in any transported quantity induce small fluctuations upon other transported quantities. Typically, these fluctuations occur at high frequencies and relatively small quantities. The computing resources that would be required to handle such frequencies are superfluous in terms of practical engineering simulations. Hence, an ideal flow model is one that reduces computing loads in comparison to the exact model and maintains the integrity of the solution. Current methods remove the small scales by time-averaging, ensemble-averaging, or otherwise manipulating the governing equations of the physical phenomena. As a result, a modified set of equations are created, and solving the set of equations requires much less computer resources than solving the exact equations. However, the modified equations contain additional unknown variables. In order to determine these variables, turbulence models are necessary.

Two-equation models are among the simplest of turbulence models for which the solution to two separate transport equations can be determined. There are several models available. However, the standard k-ε has become one of the most widely used models. The standard k-ε model is a semi-empirical model that

describes the turbulence of the kinetic energy (k) and its rate of dissipation (ε).

The derivation of the k-ε model assumes that the fluid flow is fully turbulent, and

the effects of the molecular viscosity are negligible. Thus, the k-ε model is only

valid for fully turbulent flows.

The two transport equations for the standard k-ε model are listed below.

The first equation is the turbulent kinetic energy equation (k), which is expressed

as follows:

$$\frac{\partial(\rho\kappa)}{\partial t} + \nabla(\rho\kappa\vec{V}) = \nabla\left[\left(\mu + \frac{\mu_t}{\sigma_k}\right)\nabla k\right] + G_k + G_b - \rho\varepsilon - Y_M + S_k \tag{29}$$

The second equation is the dissipation equation (ε), which is expressed as

follows:

$$\frac{\partial(\rho\varepsilon)}{\partial t} + \nabla(\rho\varepsilon\vec{V}) = \nabla\left[\left(\mu + \frac{\mu_t}{\sigma_k}\right)\nabla\varepsilon\right] + C_{1\varepsilon}\frac{\varepsilon}{k}(G_k + C_{3\varepsilon}G_b) - C_{2\varepsilon}\rho\frac{\varepsilon^2}{k} + S_\varepsilon \tag{30}$$

The turbulent viscosity, (μ_t), is evaluated using the following equation:

$$\mu_t = \rho C_\mu \frac{k^2}{\varepsilon} \tag{31}$$

The model-constants in each of the three equations above have the

following default values in Fluent:

$$C_{1\varepsilon} = 1.44$$
$$C_{2\varepsilon} = 1.92$$
$$C_\mu = 0.09$$
$$\sigma_k = 1.00$$
$$\sigma_\varepsilon = 1.30$$

These default values have been developed from studies of turbulent shear flow of water and air. These values are widely accepted among professional engineers for most applications.

CHAPTER 4
FLUENT AND NUMERICAL MODELING

The systems of governing equations that describe the motion of the fluid flow within a helically-finned tube are mathematically complex, and no known method of solving them in closed-form exists. Nevertheless, the governing equations are still useful and applicable. Numerical techniques have been developed in order to approximate the solutions to such equations. These techniques have proven to be very effective. Fluent is a computational fluid dynamics (CFD) software that implements numerical methods to solve various types of fluid flow and heat transfer problems. Fluent was the CFD that was used in this thesis. However, solving such problems requires more than a numerical solver. There are a considerable number of necessary principles and advanced computer hardware that enable Fluent to solve physical problems properly and accurately. Several of the dominant principles and computing hardware that were used to simulate and study the fluid flow within a helically-finned tube are discussed in the following sections.

4.1   <u>Computational Fluid Dynamics</u>

Ansys Fluent, or Fluent for short, is state-of-the-art CFD software that is primarily used to model fluid flow and heat transfer problems of complex geometries. For this thesis, only the fluid flow capabilities of Fluent were used.

The computer code that comprises Fluent software is written in C programming language and employs numerical algorithms that are based on the finite volume method of solving physical problems.

The finite volume method is a numerical technique that is used to represent and evaluate a system of partial differential equations in the form of algebraic equations. In terms of modeling the fluid flow within a finned tube, approximate solutions to the systems of governing equations are calculated at discrete points on a geometric mesh that represents the fluid of the physical problem. The meshed geometry of the fluid is a discrete representation of the geometry of the fluid domain within the tube. The concept of meshing is elaborated in later sections of this chapter. Together, the terms *finite* and *volume* refer to a small volume that surrounds each of the nodal points that comprise a mesh. Implementing the finite volume method to solve a problem entails several mathematical steps. First, the volume integrals that contain a divergence term in the partial differential equation are transformed into surface integrals. This transformation requires the use of Gauss' theorem, which relates the flux of vector field through a surface to the vector field inside a surface. Lastly, the surface integrals are evaluated as fluxes at the surfaces of each finite volume of the fluid domain. One of the advantages of the finite volume method is that the method is conserved. The flux entering the surface of a volume is equal to the flux leaving the surface of the adjacent volume. Consequently, the finite volume method is an ideal solution technique to be used by Fluent. As previously discussed, Fluent is based on the laws of conservation.

4.2   <u>Methodology</u>

In order to simulate the fluid flow within a helically-finned tube using Fluent, a specific order of steps was followed. The general procedure that was used in this thesis is similar to most types of CFD simulations. This procedure is outlined in the following sequence of steps:

1. A geometric representation of the fluid domain within the helically-finned tube was created using a computer aided design software package (CAD).
2. An appropriate modeling technique that would be advantageous to the solution process was chosen. However, in this thesis, three modeling techniques were considered and used to simulate the same physical problem.
3. The geometric representation of the fluid domain was divided into discrete cells using techniques to mesh the geometry.
4. The physical properties of the fluid and the boundary conditions were defined and programmed into the solver.
5. Using the solver, the governing equations of the fluid flow were solved with an appropriate model of physical flow.

In order to complete the simulation process previously outlined, three distinct types of software were needed: a preprocessor, a solver, and a postprocessor. The preprocessors that were used to create the geometry and geometric mesh of the fluid domain within the tube were SolidWorks and Gambit, respectively. Fluent was the numerical solver that was used to define the physical model, apply boundary conditions, and numerically solve the governing equations. One of the features of Fluent is that the software contains a

postprocessor, which was used to analyze the solution data and visualize the results of the simulation. Regardless of the physical problem or modeling technique, the types of software previously mentioned are always required to build, solve, and analyze a simulation.

4.3   <u>Preprocessors and Modeling Techniques</u>

As previously stated, the preprocessors that were used to create a geometric representation and a corresponding mesh of the fluid flow within a helically-finned tube were SolidWorks and Gambit, respectively. By using both software in tandem, a geometric representation of the fluid was created and divided into discrete cells using several meshing techniques. Since SolidWorks is so common, a discussion of the software is not presented. However, the functions and features of the less popular software Gambit are worth discussing.

Gambit is a geometric modeling and grid generation tool that is primarily designed to build and mesh physical models for Fluent, such that Fluent can analyze and solve the simulations. Although most physical models can be directly built in Gambit, some models are more easily created and manipulated using outside CAD programs such as SolidWorks, and Gambit supports the option of importing models from other CAD software. However, models do not always import into Gambit properly. Thus, Gambit offers a variety of options for geometry clean-up, or repair, and decomposition in order to reconstruct and rebuild the model.

In addition to building the geometry of a model, Gambit offers a wide assortment of tools for meshing a model. A user can have Gambit automatically mesh surfaces and volumes of a model while having limited control of the meshing scheme through the use of sizing functions and boundary layer meshing options. Alternatively, a model can be meshed using more rudimentary meshing tools which allow for more control of the meshing scheme. Nevertheless, the appropriate meshing tool and meshing technique depend on the modeling technique that is used to model the physical problem.

In order to model the fluid flow within the helically-finned tube, three distinct modeling techniques were used. The different techniques were used for the following reasons:

- To investigate the accuracy of each modeling technique
- To investigate the effects of mesh density
- To investigate the efficiency of the technique with respect to computing time

The three modeling techniques that were used to model the fluid flow in a helically-finned tube were the long tube model, mapping model, and periodic model. The names of the modeling techniques are ambiguous and were arbitrarily chosen. However, a detailed description of each of the techniques is provided in the next three sections.

4.3.1 Long Tube Model

The helically-finned tube that was investigated had the geometric parameters that are displayed in Table.4.1.

Table 4.1   Helically-Finned Tube Parameters.

Fin Pitch	Fin Height	Helix Angle	Included Angle	Internal Diameter	Fin Width at Tip	Fin Width at Base	Number of Starts
p	e	α	β	D	t_{tip}	t_{base}	N_s
(mm)	(mm)	(°)	(°)	(mm)	(mm)	(mm)	-
10.54	0.38	25	41	15.64	0.2	0.48	10

In order to simulate the fluid flow within the tube, a 3-dimensional model of the fluid domain was created using SolidWorks. The actual tube was not incorporated into the model since it was not a necessary part of the simulation process. The model was created using the axial profiles of the fins. After the contours of the fin profiles were created along the axial direction of the tube, the 'sweep' and 'helix' features of SolidWorks were used to create the 3-dimensional representation of the fluid domain. In order to keep the file size of the model manageable and reduce the amount of clean-up required after importing the model into Gambit, a fluid domain of only one 360° rotation of the fins, or 105.4mm of pipe length, was created. The SolidWorks model of the fluid domain is illustrated in Figure 4.1. The model was purposely designed to consist of ten separate volumes and a hollow core along the axial direction in order to facilitate better control over the meshing scheme that was used to mesh the model. After the SolidWorks model was created, it was saved as a 'parasolid' file and imported into Gambit.
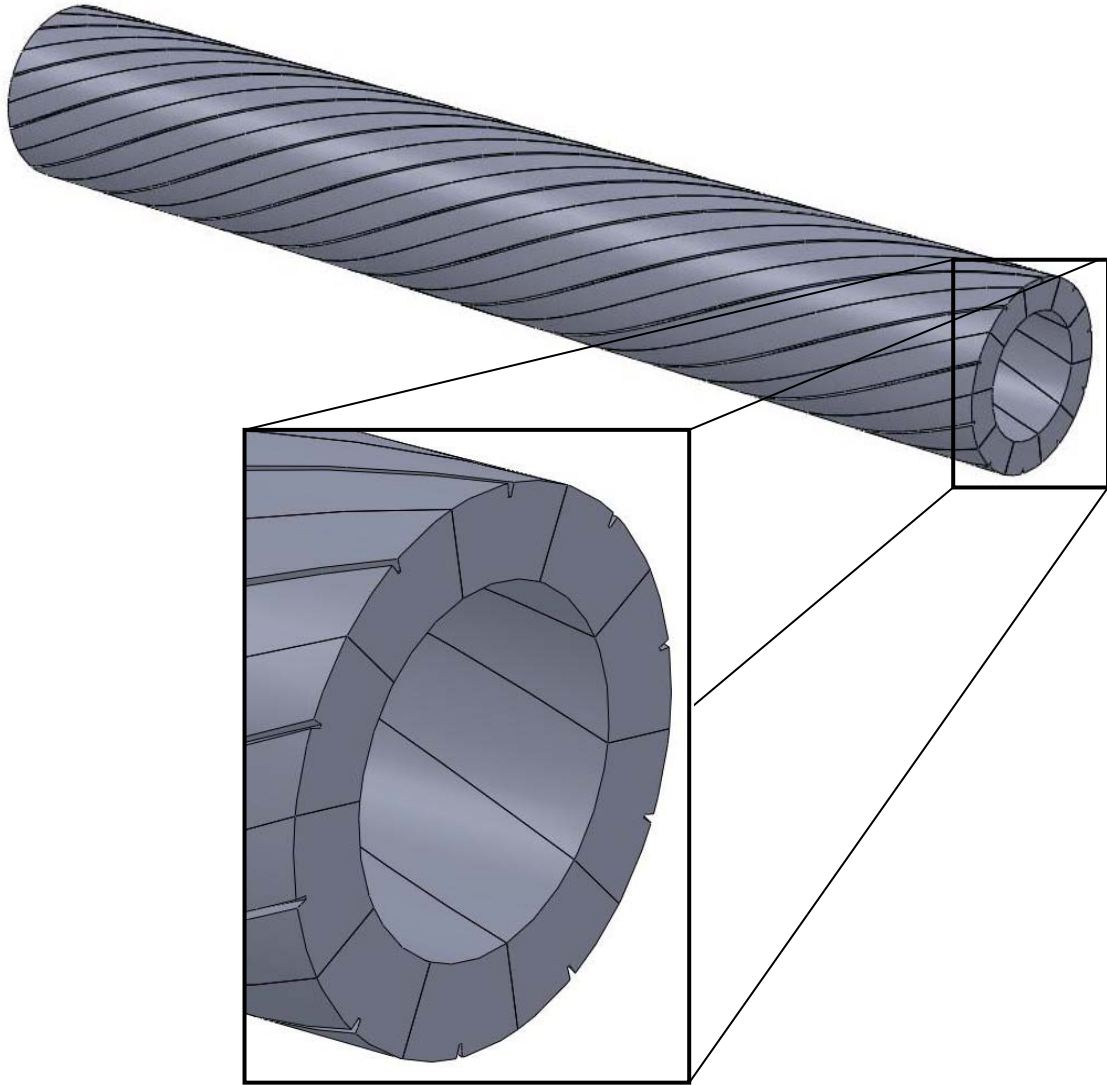
Figure 4.1.   SolidWorks Model of the Fluid Domain – Long Tube Model.

After the model was successfully imported into Gambit, it was cleaned up in order to create a continuous fluid domain. First, all of the points, lines, and faces were connected using the 'connect' feature of Gambit. After verifying that the connections were successful, an eleventh volume was created out of the hollow core along the axial direction of the model. The Gambit model of the fluid

domain is illustrated in Figure 4.2. After the eleventh volume was created, the

model was ready to be meshed.
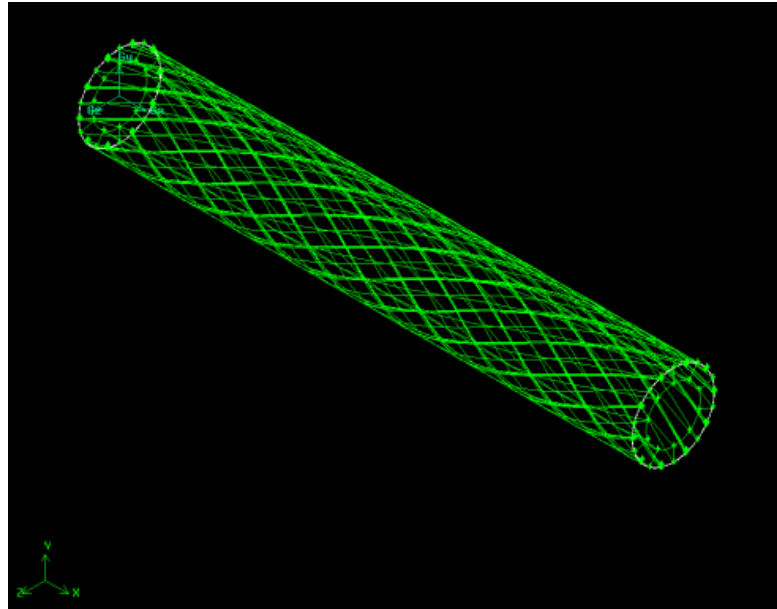
Figure 4.2.   Gambit Model of the Fluid Domain – Long Tube Model.

The meshing procedure was started at both ends of the model. Each

group of symmetric edges was meshed identically with the same number of

meshes and interval distances. After each of the edges was meshed, a boundary

layer mesh was created around the immediate perimeter of each end in order to

account for a boundary layer near the wall of the fluid model. A view of the

boundary layer mesh is illustrated in Figure 4.3. After the boundary layer mesh

was created around the entire perimeter, the faces that comprised the two ends

were meshed using the 'paving' feature of Gambit. After each of the faces was

meshed, each of the volumes was meshed using the 'cooper' feature.
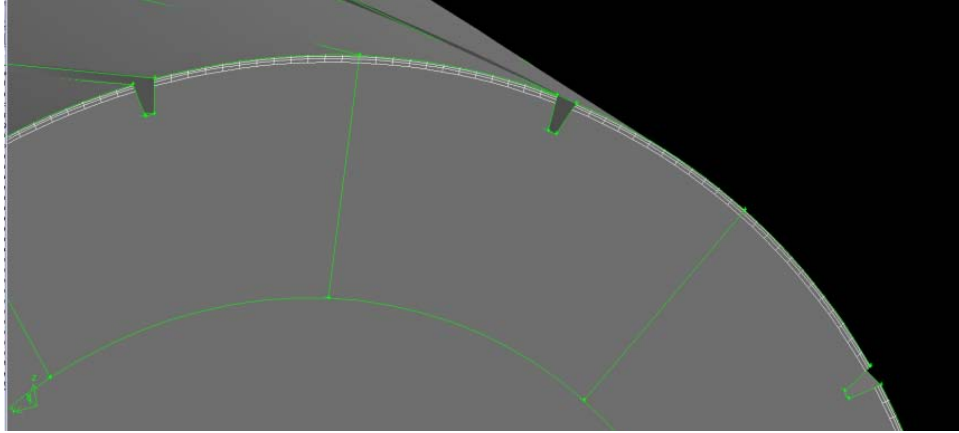
Figure 4.3.   Boundary Layer Mesh – Long Tube Model.
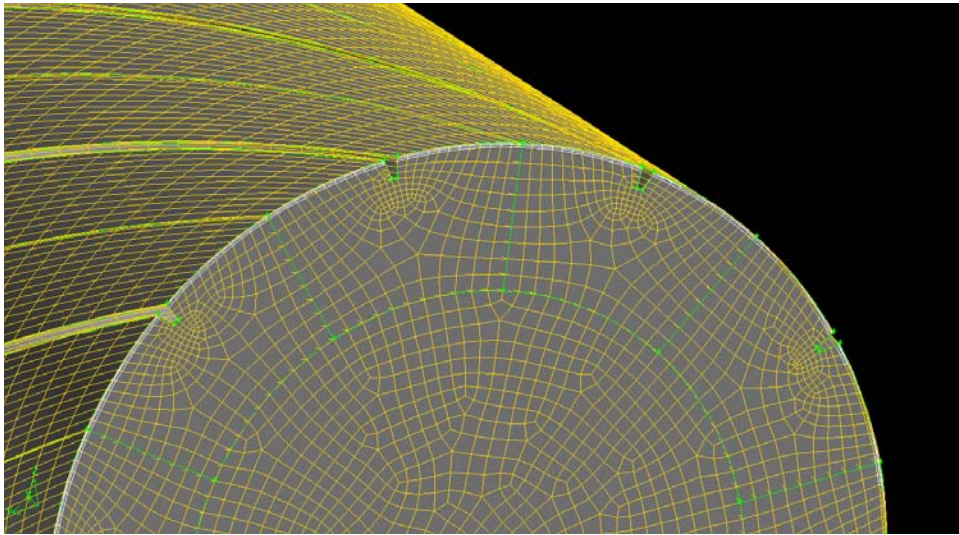
Figure 4.4.   Volume Mesh of the Fluid Domain – Long Tube Model.

The final steps of creating the long tube model were to 'copy-and-move' the one-cycle mesh previously created in order to create a longer model and to assign boundaries to the model. Using the 'copy-and-move' feature of Gambit, the one-cycle mesh was copied and moved eleven times in a sequential fashion along the axial direction. In order to create one continuous model from the eleven copies, the copied adjacent points, edges, and faces were connected using the

'connect' feature of Gambit. Subsequently, the total length of the model was 1.1594 m. The entire model is illustrated in Figure 4.5. Finally, the circumferential faces of the model were defined as 'walls', the inlet and outlet of the model were labeled as a 'velocity-inlet' and 'exit', respectively, and the domain of the model was defined as 'fluid'. Finally, the model was ready to be solved in Fluent using the long tube modeling technique.
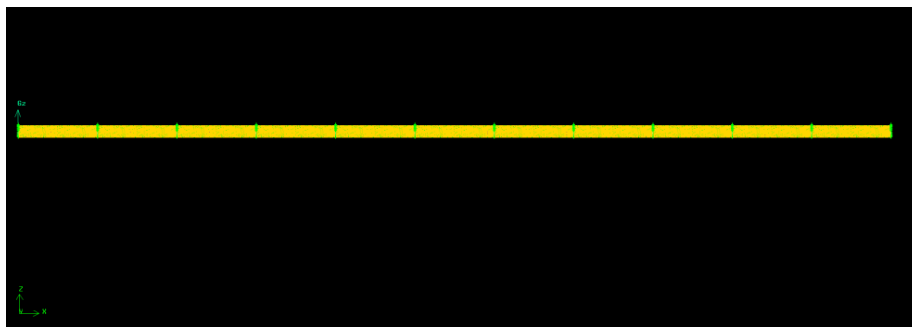
Figure 4.5.   Volume Mesh of the Fluid Domain – Long Tube Model.

The long tube modeling approach is a technique of modeling the fluid flow along a sufficient length of tube such that the flow becomes fully developed before the exit region of the flow model. This model assumes a uniform velocity flow at the inlet, and the flow develops fully along the length of the tube. As the flow becomes fully developed near the exit, a linear pressure drop can be measured. A corresponding friction factor can be calculated from the linear pressure drop.

4.3.2   Mapping Model

The 3-dimensional model that was created for the mapping model was developed in a similar fashion as the long tube model. However, only one

complete cycle of the rib pattern was necessary for this modeling technique. As outlined in the previous section, a 3-dimensional model of the fluid domain within the helically-finned tube was created in SolidWorks using the tube dimensions that are displayed in Table 4.1. Initially, the primary geometries of the model were created in SolidWorks, and the model was imported into Gambit. After the model was imported, it was cleaned-up and made into one continuous model. A boundary layer mesh was created about the immediate outer perimeter of the model. After creating the boundary layer mesh, the entire model was fully meshed, and the boundaries and the fluid domain were defined in Gambit. An illustration of the meshed model is shown in Figure 4.6. Finally, the model was ready to be solved in Fluent using the mapping modeling technique.
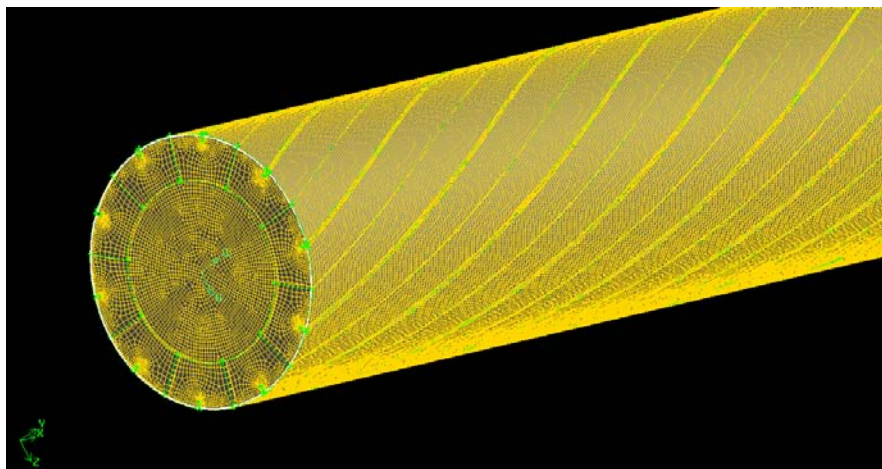
Figure 4.6.   Volume Mesh of the Fluid Domain – Mapping Model

The mapping modeling technique is a multi-step process of solving a series of models. Recall that the fluid mesh of this technique consists of only one rib-cycle. Hence, the mapping model was much smaller than the long tube model and less cumbersome, computationally. Initially, a uniform velocity flow was

47

assumed at the inlet, and the flow developed slightly along the length of the model (one cycle). After the model was solved, a solution existed at the exit of the model, which consisted of the x-velocity, y-velocity, z-velocity, turbulence-dissipation-rate, and turbulence-kinetic-energy. The software stored these values at each of the nodes of the faces that comprised the exit. The values were then saved in file format and mapped back to the inlet condition of the model by reintroducing the values as 'velocity-inlet' conditions. Hence, the solution at the exit of the original model became the initial condition of the successive model. The model was then solved again in Fluent. This procedure was repeated until the flow became fully developed. Once this process was completed, a linear pressure drop could be measured, and the friction factor was calculated.

4.3.3   Periodic Model

The model of the fluid domain that was created for the 'periodic model' was done so in a similar fashion as the long tube model and the mapping model. For this modeling technique, only one complete cycle of the rib pattern needed to be constructed. The model of the fluid domain was created using the helically-finned tube dimensions that are displayed in Table 4.1. The primary geometries of the model were created using SolidWorks, and the model was created from the axial profiles of the fins. After creating the contours of the fin profiles along the axial direction of the tube, the 'sweep' and 'helix' features of SolidWorks were used to create the 3-dimensional representation of the fluid domain. Initially, 11 independent volumes were created. However, the 11 volumes were merged into one single volume using the 'merge' feature of SolidWorks. Only one 360°

rotation of the fins, or 105.4mm of pipe length, of the fluid domain was created. The SolidWorks model of the fluid domain is illustrated in Figure 4.7. After creating the SolidWorks model, the model was imported into Gambit for meshing.
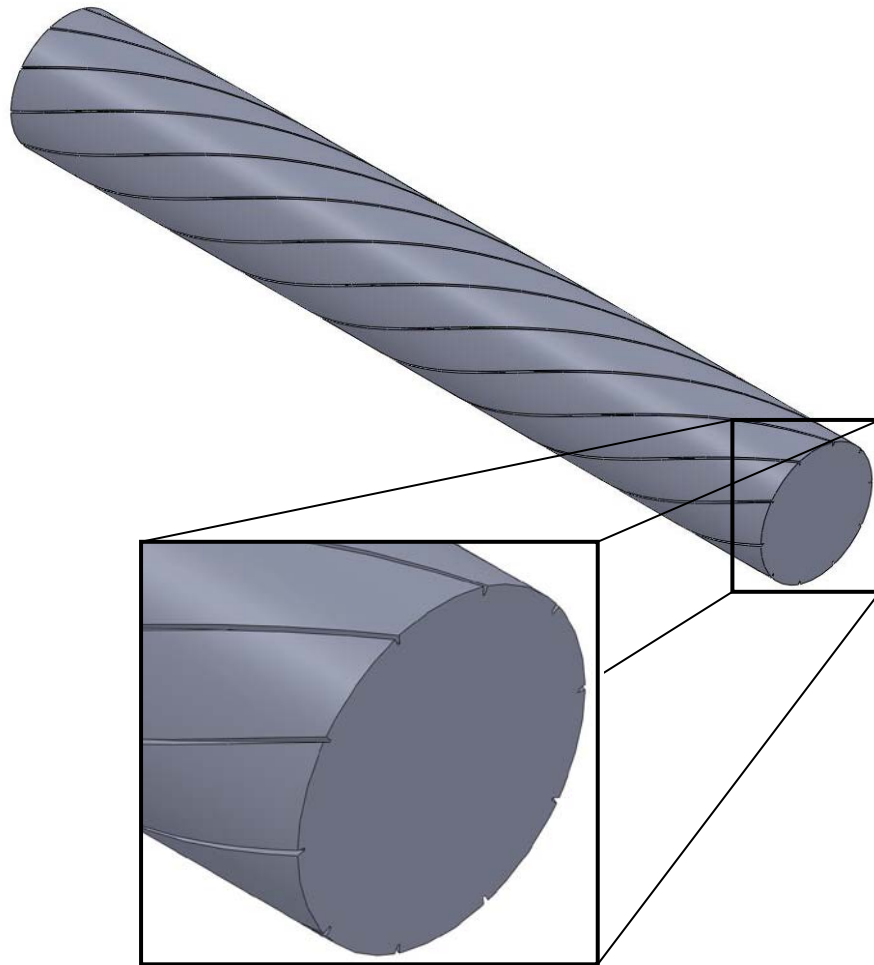
Figure 4.7.   SolidWorks Model of the Fluid Domain – Periodic Model.

After the model was imported into Gambit, it was cleaned-up and made continuous by connecting all of the adjacent points, lines, and faces using the 'connect' feature of Gambit. Next, a boundary layer mesh was constructed along the immediate outer perimeter of the fluid domain. The boundary layer mesh is

illustrated in Figure 4.8. After the boundary layer mesh was created, the axial-front and axial-back faces of the model were 'hard-linked' and meshed using the 'paving' feature. The volume of the model was meshed using the 'cooper' feature of Gambit. The meshed model is illustrated in Figure 4.8. Finally, the circumferential faces of the model were defined as 'walls', the two faces perpendicular to the axial direction were defined as 'periodic boundaries', and the domain of the model was defined as 'fluid'. Finally, the model was ready to be solved using the periodic modeling method in Fluent.
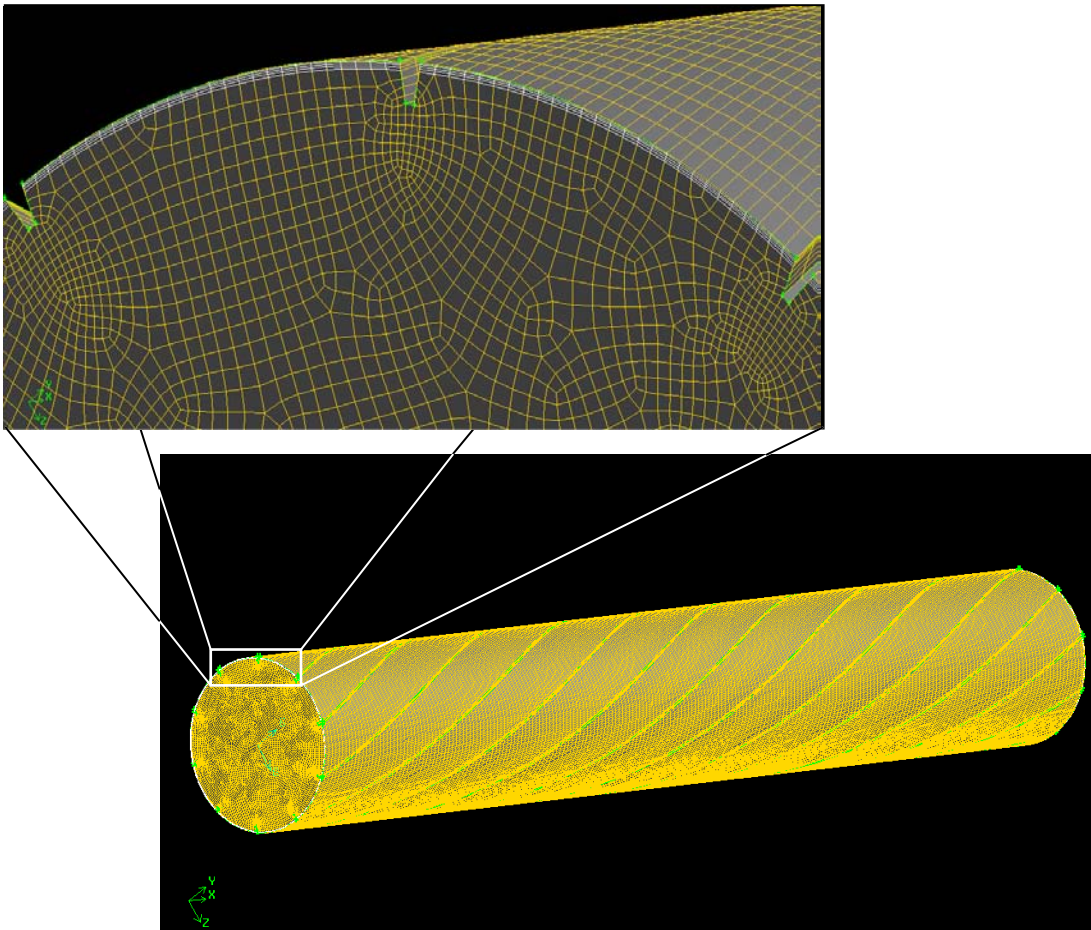
Figure 4.8.   Boundary Layer and Volume Mesh of the Fluid Domain – Periodic Model.

The periodic modeling technique is based on periodic boundary conditions, which are described as boundaries within a physical problem where the geometry and the flow pattern of a model behave in a periodically repeating fashion. The periodic boundary conditions are applicable when the fluid flows, which are across two planes that are opposite of one another, are identical. Periodic boundaries or planes are always coupled. Fluent treats the flow at one periodic boundary as though the other periodic boundary is adjacent to the first. Since the fluid flow within a helically-finned tube is expected to repeat in a periodic fashion along the axial length of the tube, the periodic boundary conditions seems to be an appropriate modeling technique. As Fluent solves a periodic model, the software calculates the pressure drop that occurs between the coupled boundaries from which the friction factor can be calculated. The mathematical justification for periodic boundary conditions is presented in the next section.

4.4 Periodic Boundary Conditions

The basic assumption of periodicity is that the velocity components of a flow repeat in space over some length, *L*. This assumption can be stated mathematically as follows:

$$u(\vec{r}) = u(\vec{r} + \vec{L}) = u(\vec{r} + 2\vec{L}) = \cdots \qquad (32)$$

$$v(\vec{r}) = v(\vec{r} + \vec{L}) = v(\vec{r} + 2\vec{L}) = \cdots \qquad (33)$$

$$w(\vec{r}) = w(\vec{r} + \vec{L}) = w(\vec{r} + 2\vec{L}) = \cdots \qquad (34)$$

51

In order to illustrate the periodic properties of a flow, consider the 2-dimensional tube bank problem that is illustrated in Figure 4.9 and the mathematical relationships that follow thereafter.
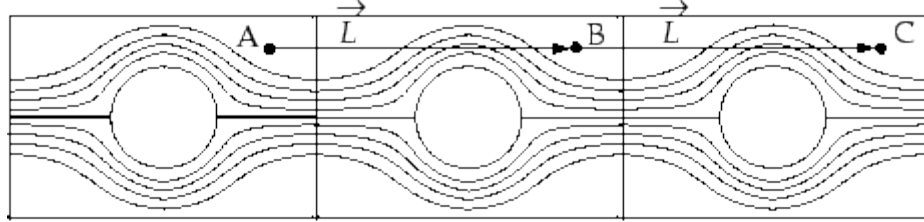
Figure 4.9.   Periodic Flow over a Tube Bank [Fluent Inc. (2006)].

$$u_A = u_B = u_C \qquad \tilde{p}_A = \tilde{p}_B = \tilde{p}_C$$

$$v_A = v_B = v_C \qquad \tilde{p}_A - \tilde{p}_B = \tilde{p}_C - \tilde{p}_B$$

However, the periodicity of the pressure for a viscous flow is different in the sense that the pressure drop is periodic between the periodic boundaries. Mathematically, the periodic pressure drop between the periodic boundaries can be written as follows:

$$\Delta p = p(\vec{r}) - p(\vec{r} + \vec{L}) = p(\vec{r} + \vec{L}) - p(\vec{r} + 2\vec{L}) = \cdots \qquad (35a)$$

With respect to a pressure based solver, which is discussed in the next section, the local pressure gradient can be decomposed into two separate components. The first component is the gradient of the periodic component, $\nabla \tilde{p}(\vec{r})$, and second component is the gradient of the linearly-varying component, $\beta \vec{L}/|\vec{L}|$. Hence, the local pressure gradient can be written as:

$$\nabla p(\vec{r}) = \beta \frac{\vec{L}}{|\vec{L}|} + \nabla \tilde{p}(\vec{r}) \qquad (35b)$$

In Equation (35b), $\tilde{p}(\vec{r})$ is the periodic pressure, which is pressure that remains after the linearly-varying pressure, $\beta|\vec{r}|$, is subtracted from the local pressure. The linearly-varying component of the local pressure is the result of a force that acts on the fluid in the governing momentum equation. However, the value of β is not known beforehand. Thus, the value of β is iterated upon during the pressure correction step of the solving algorithm. The iteration continues until the intermediate mass flow rate of the iteration matches the mass flow rate that was defined by the model. Hence, the periodic model requires sub-iterations within the usual iterations that Fluent uses to solve a model.

4.5   Pressure-Based Segregated Algorithm

There are two types of flow solvers that Fluent uses to numerically solve a model: a pressure-based solver and a density-based solver. Typically, the pressure-based solver is used to solve low-speed incompressible flows, and the density-base solver is used to solve high-speed compressible flows. The pressure-based solver was used to model the flow within a helically-finned tube, which is the focus of this thesis.

The pressure-based solver is based on an algorithm that numerically solves the governing equations of a flow in a segregated, sequential fashion, or, equivalently, each of the governing equations is solved separately, one after another. As noted in the previous chapter, the governing equations of a fluid flow are non-linear partial differential equations and coupled. Subsequently, the numerical solution to the governing equations, or the model, requires iterative

53

calculation loops. The iterative process that is performed with the pressure-based

solver is outlined in Figure 4.9. Initially, 'Update properties' consists of the initial

conditions of the model, after which it becomes the solution of the previous

iteration. Next, the momentum equations are solved sequentially, using updated

values, and the pressure correction equation is solved using the updated values

of the pressure and face mass fluxes. Afterwards, the pressure correction is used

to correct the velocity field, mass fluxes, and pressure. Next, the equations are

solved for any additional scalars, such as turbulent quantities and energy. Finally,

the convergence criteria of the solution are checked, and the iterative loop

continues to cycle until the convergence criteria are satisfied.
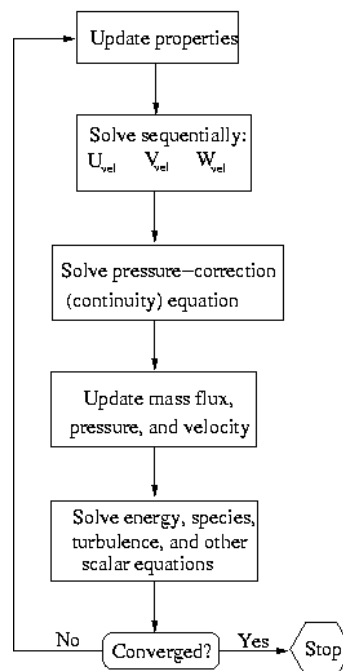
Figure 4.10. Pressure-Based Segregated Algorithm [Fluent Inc. (2006)].

54

4.6   Discretization

As previously described in section 4.1, Fluent uses a finite control volume analysis to solve a model. This technique entails integrating each of the governing equations about each volume or volume-mesh and creating discrete equations that satisfy the laws of conservation. The original governing equations of the flow are thus transformed into a system of equations that can be solved with numerical methods. This process is referred to as *discretizing* the governing equations. This process is illustrated in Equation (36), which is the equation of the steady-state conservation of transport with respect to the scalar quantity φ over a control mesh volume V_m.

$$\oint \rho\varphi\vec{v} \cdot d\vec{A} = \oint \Gamma_{\varphi}\nabla\varphi \cdot d\vec{A} + \int S_{\varphi}dV_m \tag{36}$$

Equation (36) can be discretized for any given volume-mesh in the following fashion:

$$\sum_{f}^{N_{\text{faces}}} \rho_f\overrightarrow{v_f}\varphi_f \cdot \overrightarrow{A_f} = \sum_{f}^{N_{\text{faces}}} \Gamma_{\varphi}(\nabla\varphi)_{\text{n}} \cdot \overrightarrow{A_f} + S_{\varphi}V_m \tag{37}$$

As a default setting, Fluent stores the discrete values of φ at the centers of each volume mesh. However, the face values φ_f are required in order to determine the convection terms in Equation (37). In order to determine the face values, an interpolation method is used. This computation interpolates using the values from

the centers of the volume meshes. This interpolation calculation is accomplished using an upwind scheme.

For the model of the flow within the helically-finned tube that is examined in this thesis, the second-order upwind scheme was used in Fluent. By selecting this numerical scheme, the values at the faces of the volume meshes are calculated with a multidimensional linear reconstruction approach where higher-order accuracy is achieved at each face using a Taylor series expansion of the volume mesh-centered solution about the centroid of each mesh.

4.7   Linearization

Part of the process of solving a model using a segregated solution method is making the discrete, non-linear governing equations of a flow linear. In doing so, a solvable system of equations for the dependent variables of each of the governing equations is created for every computational mesh of the model. Thus, each of the discrete equations is transformed into a linear equation implicitly with respect to the dependent variables in each one. In order to solve the new system of equations, a point implicit (Guass-Seidel) linear equation is used along with an algebraic multi-grid method to solve the system for the dependent variable in each computational mesh.

4.8   Convergence Criteria

When trying to determine whether or not the solution of a model is complete, there are several solving factors that should be considered. Some examples include: flow development, overall balances, residual reports, and

force monitors. A residual report is one of the most referenced factors when determining the completeness of a solution. This is due to the inherent nature of the solution process that is used to solve CFD problems.

As discussed in previous sections, Fluent solves a model by solving a system of non-linear partial differential equations using iterative numerical techniques. During this process, an approximate solution is obtained at each iterative, computational step, and there is a corresponding error associated with each approximation. The error results from a small imbalance, or residual, in the governing equations. As the iterative process continues, the residuals tend to decrease and converge toward some relatively small number under normal circumstances. As the residuals converge toward some relatively small number in a decreasing fashion, the corresponding error with respect to the previous iteration decreases as well. If the residuals no longer change with successive iteration, the solution is said to have absolutely converged. However, absolute convergence is not always necessary or practical. Often, a less stringent set of conditions is sufficient. Such conditions are referred to as convergence criteria, which are defined as a pre-set of conditions on the residuals that indicate a certain level of convergence has been obtained.

Unfortunately, there is no definitive number that indicates absolute convergence or a good solution. Fluent uses the default value 10^{-3} for the convergence criteria of each governing equation except for the energy equation. The default value for the energy equation is set at 10^{-6}. However, the convergence criteria were set to be at most 10^{-5} for each of the equations with

respect to the models that are considered in this thesis. In addition to convergence criteria, other factors were considered in determining the completeness of the solutions of the models.

4.9   Parallel Processing in Fluent

When solving a model with Fluent, a single processor or multiple processors may be used. On a single computer (one processor), the Fluent serial solver is responsible for managing file input and output, data storage, and flow field calculations. The serial solver manages such data using a single solver process. The serial architecture that Fluent uses is illustrated in Figure 4.11.
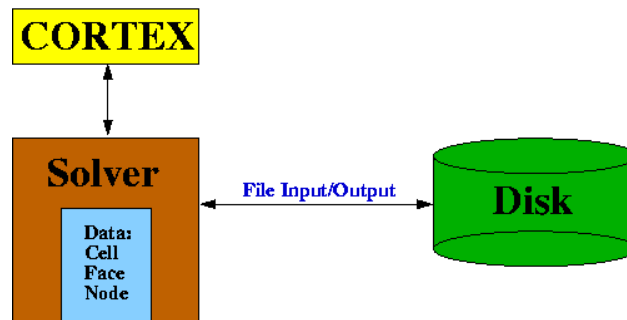
Figure 4.11.   Serial Fluent Architecture [Fluent Inc. (2006)].

Fluent also allows a user to solve a model using multiple processors. Solving a model with multiple processors is referred to as parallel processing. Parallel processing is a joint interaction between Fluent, a host processor, and a set of computer-node processors. Using a utility called a cortex to manage the user interface and basic graphical functions, Fluent interacts with the host processor and the collection of computer-nodes. The parallel architecture of Fluent is illustrated in Figure 4.12.
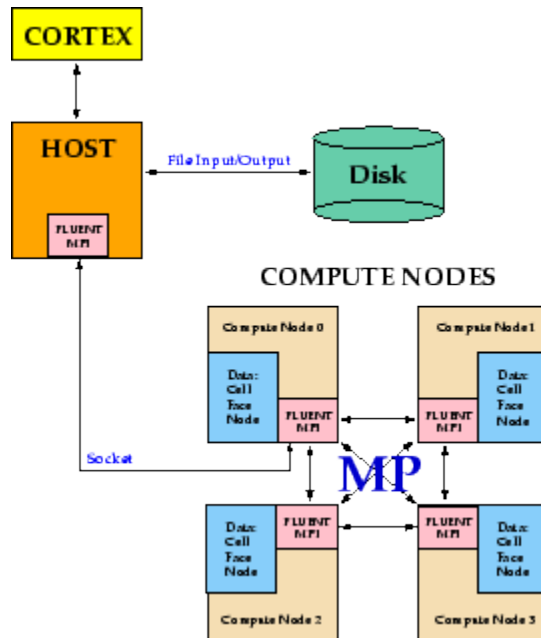
Figure 4.12. Parallel Fluent Architecture [Fluent Inc. (2006)].

When a model is solved using parallel processors, Fluent divides the mesh and the corresponding data into multiple partitions. After the mesh is split up, Fluent assigns each partition to a different compute process, or node. Finally, Fluent solves each partition independently on each node and reassembles the solution after each partition has been solved. The process of partitioning is discussed in greater detail in Section 4.11.

4.10   Linux Cluster

In order to perform the Fluent analysis of the models of the fluid flow within a helically-finned tube for this thesis, a Linux cluster computer system was used. The Linux cluster was provided by the Babcock & Wilcox Company (B&W). The Linux cluster was used for two primary reasons. First, a conventional laboratory

computer did not have the capacity to handle the large data files of the models. Secondly, the cluster offered the use of parallel nodes. Solving the models on parallel processors greatly reduced the computing time. The Linux cluster provided by B&W has the following specifications:

- 1 x File Server
  - 1 DualCore 2.6Hz CPU, 2GB RAM, 2 x 36GB SCSI
  - 1 x 4Gb Infiniband HCA, 2 x 4GB FC HBAs, 5.1TB SAN
- Head Node
  - 1 DualCore 3.0GHz CPU, 16GB RAM, 2 x 36GB SCI
  - 1 x 4GB Infiniband HCA
- 20 x Compute Nodes
  - Each with 2 DualCore 3.0GHz CPU, 16GB RAM
  - 1 x 80GB SATA, 1 x 4 GB Infiniband HCA
- 4 x Compute Nodes
  - Each with 2 QuadCore 2.4 GHz CPUs, 16GB RAM
  - 1 x 80 GB Sata, 1 x 4GB Infiniband HCA

The Fluent models for this thesis were solved using only two nodes in parallel on the group of 20-x-Compute-Nodes with a 2 DualCore, 3.0GHz processor, and 16GB of RAM. Using two nodes, the computing time was reduced by half with respect to using only a single node.

4.11 <u>Grid Partitioning</u>

Grid partitioning is a method of subdividing a mesh into groups of cells that can be solved simultaneously on separate processors. This feature was used to solve the helically-finned tube simulations for this thesis. The mesh of the fluid domain of the finned tube was partitioned into two groups and solved on

parallel processors so that the computing time associated with the simulation was reduced by half of the original computing time using only one processor. Fluent offers two types of partitioning options. The first option is an automatic partitioning algorithm that is used to read an un-partitioned grid into a parallel solver, whereas the second option is a manual partitioning technique that is read into a serial solver. The user manual of Fluent suggests using the automatic partitioning algorithm for large grids. Due to the size of the fluid mesh of the finned tube models, the grids of the fluid domain were partitioned using the automatic partitioning option and read into a parallel solver.

The partitioning algorithm that Fluent uses for parallel solvers has three primary functions built into the algorithm. The first function is to create the partitions such that there are an equal number of cells in each partition. Creating an equal number of cells ensures that each processor is given an equal load of cells to solve, and the partitions are ready to communicate with one another at the end of the solving process at approximately the same time. The second and third functions of the algorithm are designed to minimize the number of partition interfaces and partition neighbors. By minimizing the number of partition interfaces, the time required by the computer to communicate information between the partitions is minimized, too.

4.12   Journal Files

In order to solve a Fluent model on the Linux cluster that was used for this thesis, a journal file was needed. A journal file is text file that contains a series of text user interface commands (TUI) that are read into Fluent and executed. The

journal files that were created for the Fluent models of this thesis were used to

execute Fluent commands on the Linux cluster. Furthermore, the journal files

were used to simplify repetitive modeling tasks that were required for the

mapping modeling technique.

CHAPTER 5
FLUENT SETUP

The primary data that were used to build Fluent models of a flow within a

helically-finned tube for this thesis are presented at the end of Section 2.2, where

the experimental friction results from Zdaniuk et al. (2008) are displayed. The

tube configuration properties were taken from case Tube 1. The geometry of

Tube 1 is presented in Chapter 4. Zdaniuk et al. (2008) considered 25 different

flow cases for Tube 1, and 7 of the 25 cases were modeled with Fluent for this

thesis. The models were built in Fluent using the experimental data that was

reported. However, some information that was necessary to build the Fluent

models was neither measured nor reported. Thus, several assumptions were

imposed in order to build a complete model. The necessary assumptions are

highlighted in the subsequent sections of this chapter. Using the three modeling

techniques to model each of the 7 flow cases, 21 Fluent models were built. The

data and Fluent settings that were used to model each flow case are presented

in the following sections.

5.1   Flow Data from Experiment and Assumptions

The experimental flow friction data from Zdaniuk et al. (2008) that was

used to create the Fluent models were received directly from Gregory Zdaniuk,

an author of the experiment, in the form of an Excel data file. The file contained

all of the recorded flow data (and results) that were obtained during the experiment. The Reynolds number of each flow case of the experiment is displayed in Table 5.1, along with the inlet water temperatures and the corresponding case identification numbers that were used by Zdaniuk et al. (2008). However, more information about the experimental setup was needed in order to successfully model the flows with Fluent.

Table 5.1   Experimental Flow Data from Zdaniuk et al. (2008).

Case Number	Zdaniuk et al. (2008) Identification	Reynolds Number	Inlet Water Temperature (˚C)
1	Case 1	12,206	20
2	Case 4	18,632	20
3	Case 7	24,412	20
4	Case 10	29,832	20
5	Case 13	36,292	20
6	Case 17	44,426	20
7	Case 22	54,373	20

Most of the additional information that was needed to build the models was derived from the Reynolds numbers and the tube geometries. However, other pertinent information had to be assumed. Two vital pieces of information about the fluid flow that needed to be determined were the average velocities and the mass flow rates. These were determined using Equations (38) and (39), respectively.

$$V_{avg} = \frac{Re \cdot v}{D_h} \tag{38}$$

64

$$\dot{m} = \rho A V_{avg} \tag{39}$$

With respect to V_{avg}, the hydraulic diameter was calculated using the inlet area

and the wetted perimeter of the tube model. These measurements were obtained

from the SolidWorks models using the 'Measure' feature of SolidWorks. Direct

measurements of the inlet area or the wetted perimeter were not explicitly stated

in Zdaniuk et al. (2008). Although the kinematic viscosity, ν, was not specified in

the report of the experiment, the kinematic viscosity was assumed to be

$\nu = 1.00481 \cdot 10^{-6}$ m^2/s, which is the normal kinematic viscosity of water at $20°C$,

the inlet temperature of the flow. Furthermore, the density of the water was

assumed to be $\rho = 998.2$ kg/m^3, which is the normal density of water at $20°C$.

Table 5.2 illustrates most of the necessary flow values that were used to build the

Fluent models.

Table 5.2   Input Flow Data for Fluent Models.

Case Number	Reynolds Number	Velocity	Mass Flow Rate	Hydraulic Diameter	Density	Kinematic Viscosity
-	-	(m / s)	(kg / s)	(m)	(kg / m^3)	(m^2 / s)
1	12205.6	0.8867	0.1695	0.0138	998.2	1.0048E-06
2	18631.7	1.3535	0.2587	0.0138	998.2	1.0048E-06
3	24412.3	1.7734	0.3389	0.0138	998.2	1.0048E-06
4	29832.25	2.1671	0.4142	0.0138	998.2	1.0048E-06
5	36292.4	2.6364	0.5039	0.0138	998.2	1.0048E-06
6	44425.8	3.2272	0.6168	0.0138	998.2	1.0048E-06
7	54372.53	3.9498	0.7549	0.0138	998.2	1.0048E-06

Another piece of information that was neither reported nor measured

during the experiment was the roughness height of the inner walls of the

helically-finned tubes. Nevertheless, Zdaniuk et al. (2008) reported that the tubes

were manufactured using copper-nickel material, which has a common

roughness height of $e^* = 1.5 \cdot 10^{-6}$ m (Fox). Hence, the roughness height

$e^* = 1.5 \cdot 10^{-6}$ m was assumed in each of the numerical models.

5.2   Fluent Settings

Using three different modeling techniques, there were three primary

modeling settings for each of the 7 flow cases that were modeled for this thesis.

As previously stated, the three modeling techniques include: a long tube model, a

mapping model, and a periodic model. The basic Fluent settings that were used

to implement each technique are outlined in the following sections.

5.2.1   Fluent Settings - The Long Tube Model

In order to simulate the flow of each case using the long tube modeling

technique, a similar set of Fluent settings was used for each case. The only

variable settings were the inlet velocities and the number of iterations.

Nevertheless, each model was iterated until the convergence criteria were

satisfied. The following settings, along with the journal file that was used to

execute the Fluent commands on the Linux cluster, comprised the long tube

modeling technique. These setting were used to model each of the 7 cases that

were considered in this thesis.

Solver

Type	Pressure-Based
Velocity Formulation	Absolute
Time	Steady

Model

Viscous

Model	k-epsilon (2 eqn)
k-epsilon Model	Standard
Near-Wall Treatment	Standard Wall Functions
Model Constants	$C_\mu = 0.09, C_{1\varepsilon} = 1.44, C_{2\varepsilon} = 1.44$
	$PN = 1$

Materials

water-liquid

Material Type	Fluid
Density (kg/m3)	998.2
Viscosity (kg/m-s)	0.001003

Cell Zone Conditions

Operating Conditions

Operating Pressure (Pascal)	0
Reference Pressure Location	(1.1593, 0, 0)

Boundary Conditions

Inlet

Velocity Specification Method	Magnitude and Direction
Reference Frame	Absolute
Velocity Magnitude (m/s)	0.8866
Component Flow Direction	(1, 0, 0)
Turbulent Intensity (%)	5
Hydraulic Diameter (m)	0.013832

Wall

Wall Motion	Stationary Wall
Shear Condition	No Slip

Roughness Height (m)	1.5e-06
Roughness Constant	0.5

Solution Methods

Scheme	Simple
Momentum	Second Order Upwind
Turbulent Kinetic Energy	Second Order Upwind
Turbulent Dissipation Rate	Second Order Upwind

Monitors

Residuals - Print	Residuals: 1e-05

Run Calculation   1500 iterations

In order to solve the flow cases using the Linux cluster, the Fluent case-and-data files and a journal file were submitted to the cluster in tandem. The journal file that was used to run the Fluent model on the Linux cluster is presented in Appendix A.1.

5.2.2 Fluent Settings – The Mapping Model

The necessary settings, procedure, and journal file that comprised the mapping model technique differ from the long tube modeling technique. As stated in Section 4.11, the mapping technique relies on several Fluent runs. The outlet solution is repeatedly mapped to the inlet of a successive model, and Fluent solves a new model each time the mapping process occurs. Inherently, there are two primary settings that comprise this technique. First, the model is solved with a uniform velocity at the inlet of the model, and a solution is obtained at the exit. The secondary setting is a repetitive loop of mapping the exit-solution of the fore-model to the inlet boundary condition of the successive model. The following settings are the primary settings of the mapping technique.

Solver

    Type   Pressure-Based

    Velocity Formulation   Absolute

    Time   Steady

Model

    Viscous

        Model   k-epsilon (2 eqn)

        k-epsilon Model   Standard

        Near-Wall Treatment   Standard Wall Functions

        Model Constants $C_\mu = 0.09, C_{1\varepsilon} = 1.44, C_{2\varepsilon} = 1.44$

                                            $PN = 1$

Materials

    water-liquid

        Material Type   Fluid

        Density (kg/m3)   998.2

        Viscosity (kg/m-s)   0.001003

Cell Zone Conditions

    Operating Conditions

    Operating Pressure (pascal)   0

    Reference Pressure Location   (0.1054, 0, 0)

Boundary Conditions

    Inlet

        Velocity Specification Method   Magnitude and Direction

        Reference Frame   Absolute

        Velocity Magnitude (m/s)   0.8866

        Component Flow Direction   (1, 0, 0)

        Turbulent Intensity (%)   5

        Hydraulic Diameter (m)   0.013832

    Wall

        Wall Motion   Stationary Wall

        Shear Condition   No Slip

Roughness Height (m)	1.5e-06
Roughness Constant	0.5
Solution Methods	
Scheme	Simple
Momentum	Second Order Upwind
Turbulent Kinetic Energy	Second Order Upwind
Turbulent Dissipation Rate	Second Order Upwind
Monitors	
Residuals - Print	Residuals: 1e-05
Run Calculation	900

The secondary settings of the mapping technique are slightly different from the primary settings. Namely, the inlet boundary conditions are different. The secondary settings are used repetitively until the flow becomes fully developed. The following settings are the secondary settings of the mapping technique.

Solver	
Type	Pressure-Based
Velocity Formulation	Absolute
Time	Steady
Model	
Viscous	
Model	k-epsilon (2 eqn)
k-epsilon Model	Standard
Near-Wall Treatment	Standard Wall Functions
Model Constants	$C_\mu = 0.09, C_{1\varepsilon} = 1.44, C_{2\varepsilon} = 1.44$
	$PN = 1$

Materials

    water-liquid

Material Type	Fluid
Density (kg/m3)	998.2
Viscosity (kg/m-s)	0.001003

Cell Zone Conditions

    Operating Conditions

Operating Pressure (pascal)	0
Reference Pressure Location	(0.1054, 0, 0)

Boundary Conditions

    Inlet

Velocity Specification Method	Components
Reference Frame	Absolute
Coordinate System	Cartesian (X, Y, Z)
X-Velocity (m/s)	outflow x
Y-Velocity (m/s)	outflow y
Z-Velocity (m/s)	outflow z
Turbulent Intensity (%)	5
Hydraulic Diameter (m)	0.013832

    Wall

Wall Motion	Stationary Wall
Shear Condition	No Slip
Roughness Height (m)	1.5e-06
Roughness Constant	0.5

Solution Methods

Scheme	Simple
Momentum	Second Order Upwind
Turbulent Kinetic Energy	Second Order Upwind
Turbulent Dissipation Rate	Second Order Upwind

Monitors

Residuals - Print	Residuals: 1e-05

Run Calculation	900

In order to solve the flow cases using the Linux cluster, the Fluent case-and-data files and a journal file were submitted to the cluster. The journal file that was used to run the models fully encompassed the primary settings, the secondary settings, and a repetitive solving procedure. The journal file that was used to solve the models using the mapping technique on the Linux cluster is presented in Appendix A.2.

5.2.3 Fluent Settings – The Periodic Model

The following Fluent settings, along with a journal file, comprised the periodic modeling technique that was used to model each of the 7 flow cases.

Solver

Type	Pressure-Based
Velocity Formulation	Absolute
Time	Steady

Model

Viscous

Model	k-epsilon (2 eqn)
k-epsilon Model	Standard
Near-Wall Treatment	Standard Wall Functions
Model Constants	$C_\mu = 0.09, C_{1\varepsilon} = 1.44, C_{2\varepsilon} = 1.44$
	$PN = 1$

Materials

water-liquid

Material Type	Fluid
Density (kg/m3)	998.2

Viscosity (kg/m-s)	0.001003

Cell Zone Conditions

Operating Conditions

Operating Pressure (Pascal)	0
Reference Pressure Location	(0, 0, 0)

Boundary Conditions

Periodic Conditions

Periodic Type	Translational
Type	Specify Mass Flow
Mass Flow Rate (kg/s)	0.16946
Flow Direction	(1, 0, 0)
Relaxation Factor	0.5
Number of Iterations	3

Wall

Wall Motion	Stationary Wall
Shear Condition	No Slip
Roughness Height (m)	1.5e-06
Roughness Constant	0.5

Solution Methods

Scheme	Simple
Momentum	Second Order Upwind
Turbulent Kinetic Energy	Second Order Upwind
Turbulent Dissipation Rate	Second Order Upwind

Monitors

Residuals - Print	Residuals: 1e-05

Run Calculation   6000

The journal file that was used to run the periodic models on the Linux cluster is presented in Appendix A.3.

CHAPTER 6
RESULTS AND DISCUSSION

From the discussions in the previous chapters, recall the two-part objective of this thesis. One part of the objective was to determine the performance of each of the three modeling techniques in terms of element efficiency and overall computing time that was required to complete each simulation. Two significant features of each of the three techniques were the number of mesh elements of each model and the modeling procedure of each technique. For example, the mapping modeling technique required approximately 2.9 million elements and a lengthy loop in order to solve the simulation. Such features significantly affect the computing time and the data storage space that is required to solve a model. Certainly, the most efficient modeling technique is desirable. However, the most accurate model is desirable, too.

The other part of the objective of this thesis was to numerically simulate the experimental friction results from Zdaniuk et al. (2008), tube configuration Tube 1 with Fluent. Seven flow cases from the experiment were simulated using three distinct modeling techniques. The numerical friction factor of each model was calculated using the numerical pressure drop from Fluent. The results of this thesis are presented in the following sections, along with a brief discussion of recommendations and suggestions for future work.

6.1   Mesh Elements, Computing Time, and Iterations

The corresponding meshes associated with each of the three modeling techniques consisted of varying amounts of mesh elements. The long tube model mesh was inherently long in relation to the mapping model mesh and the periodic model mesh. Quantitatively, the long tube model mesh consisted of approximately 340% more mesh elements than the periodic model and 223% more mesh elements than the mapping model. A consequence of mesh size is that a large model with many elements is computationally more expensive with respect to computing memory than a small model that consists of few elements. The number of mesh elements that comprised the meshed model of each of the modeling techniques are displayed in Table 6.1. Clearly, the long tube model required more computing memory to solve the simulation than the mapping model or the periodic model. However, the computing time that is required to solve a model can be equally, if not more, important as the computing memory requirement.

Table 6.1   Number Mesh of Elements of each Modeling Technique.

Case Number	Number of Mesh Elements		
	Long Tube Model	Mapping Model	Periodic Model
1			
2			
3			
4	6,614,850	2,970,800	1,955,028
5			
6			
7			

Two important aspects of solving models with Fluent are the amount of time that is required to solve a model and the number of iterations that are required (or satisfy the convergence criteria). The number of iterations and solving time associated with each of the modeling techniques were different. The reason for the different times and iterations was the combination of inherent Fluent-run procedures, the number of mesh elements, and the convergence criteria. The total solving time and the number of iterations associated with each of the Fluent models and modeling techniques are displayed in Table 6.2. Although the periodic models consisted of the least number of mesh elements, the periodic models generally required more iterations than the mapping models or the long tube models in order to simulate the flow.

Table 6.2   Computing Time and Iterations.

Case Number	Running Time (Hours : Minutes)			Iterations		
	Long Tube Model	Mapping Model	Periodic Model	Long Tube Model	Mapping Model	Periodic Model
1	19:36	20:33	26:09	1000	4781	6000
2	19:21	20:15	33:57	1000	4707	6000
3	27:17	20:39	35:07	1500	4853	6000
4	22:25	22:49	27:54	1200	5180	5600
5	23:32	22:32	35:04	1200	5143	6000
6	21:27	22:16	34:15	1200	5137	6000
7	21:01	26:33	34:30	1200	6125	6000

Table 6.1 and Table 6.2 show that the periodic modeling technique required up to 42% more run time than the mapping models and up to 45% more run time than the long tube models. Still, the periodic models converged very poorly, but this is discussed in greater detail in the next section. Clearly, the long

tube modeling technique and the mapping modeling technique were temporally superior to the periodic modeling technique.

As indicated by Tables 6.1 and 6.2, the solving times associated with the long tube models and the mapping models were comparable. However, the number of mesh elements that comprised the long tube models was much greater than the number of mesh elements that comprised the mapping models. Hence, solving the long tube models was computationally more expensive than solving than the mapping models. Theoretically, a slower and less expensive computer could be used to solve a flow model using the mapping modeling technique, whereas a faster more expensive computer would be required to solve a similar flow model using the long tube technique. However, the accuracy of the modeling technique was important, too.

6.2   **Fluent Results**

Recall from Section 4.8 that several solving factors of a solved Fluent model need to be examined or considered in order to determine whether a Fluent solution is complete. However, there is no universal standard for determining a solution complete, and the factors that are examined are often preferential and ambiguous. Nevertheless, various aspects of the numerical solution of each model considered in this thesis were examined in order to determine the validity of the models. Primarily, the residual reports of each model and the developed velocity fields were examined. After determining that each model was indeed complete, the numerical friction factors were determined.

6.2.1 Convergence of the Long Tube Models

In order to determine that the solution of each of the long tube models was complete, four factors were examined: the residual report; the developing velocity field along the tubular model; the developing swirl number along the model; and the pressure drop along the model. Although seven long tube models were examined, all of the numerical solutions behaved in a similar fashion. Hence, only the solution factors of one model are presented.

The residual report is one of the most referenced solution factors in determining the completeness of a solution. The convergence of the solution of Case 5 is illustrated in Figure 6.1. At iteration number 1200, the residuals of the governing equations were at most 10^{-5}. Hence, the convergence criteria of the solution were satisfied, and the convergence of the residuals of the solution was considered to be satisfactory.
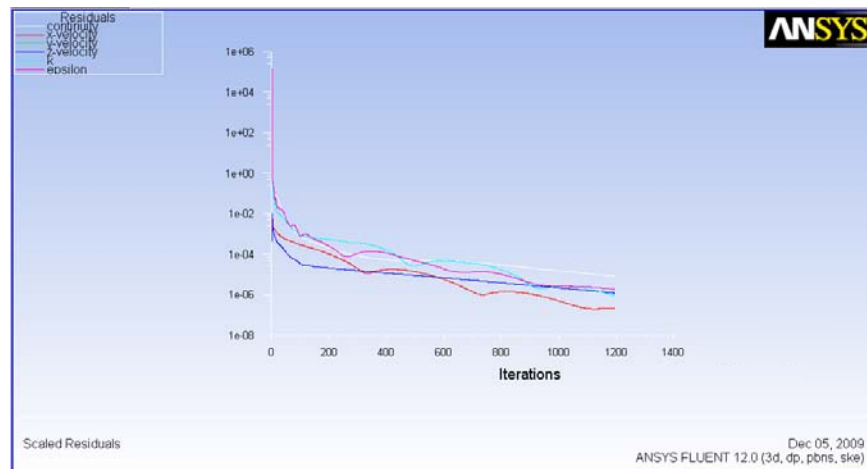

Figure 6.1.   Residual Report of Case 5 – Long Tube Model.

The velocity field along the center plane of the fluid models is another solution factor of the long tube models that was considered. As discussed in Section 5.2.1, the initial velocity at the inlet of the long tube models was constant and uniform. As a result, the flow was expected to develop as the distance from the inlet increased. Furthermore, the flow was expected to become fully developed toward the end portion of the model. At the diameter of the model, the contours of the velocity field near the inlet of the tube (Case 5) are illustrated in Figure 6.2, and the contours of the velocity field near the end of the model are illustrated in Figure 6.3. As the flow developed along the model from the inlet, the magnitude of the velocity became greatest near the center of the tube and 0 m/s at the wall of the tube, which was expected. Furthermore, the velocity contours became more stable, or developed, as the flow moved along the tube. As a result of these observations, the fluid flow appeared to be fully developed. However, the rotational aspect, or swirl, of the flow was investigated, too.
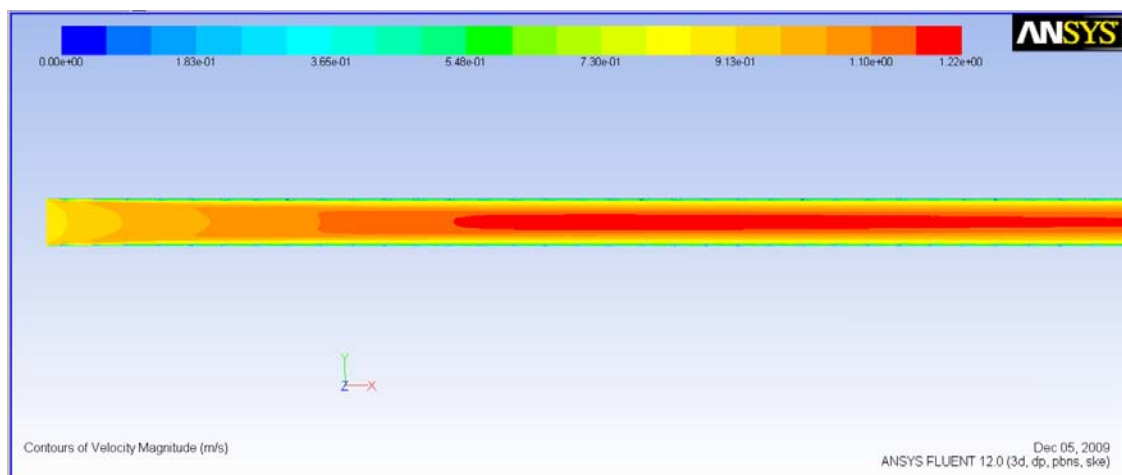

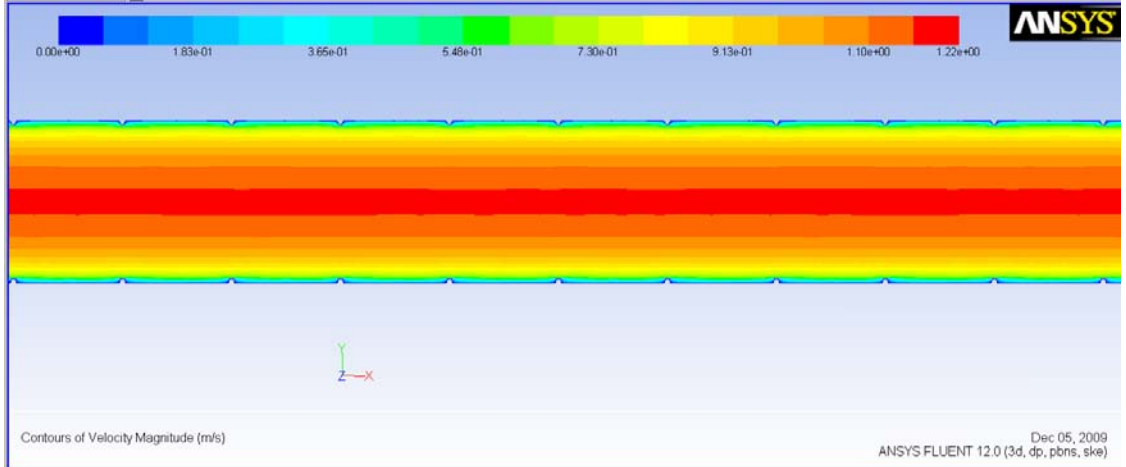Figure 6.2.   Velocity Contours at Inlet of Case 5 – Long Tube Model.

Figure 6.3.   Velocity Contours near the Exit of Case 5 – Long Tube Model.

The developing swirl number along the tube model was another solution

factor that was considered in each of the long tube models. Usually, the concept

of *swirl number* is reserved for gas jet combustion nozzles. However, the

mathematical definition of swirl number could be utilized to investigate the

development of the swirling flow along the tube and aid in determining whether

the flow near the exit was fully developed. The swirl number is defined as the

ratio of the axial flux of angular momentum and the axial flux of the axial

momentum. Mathematically, the swirl number can be defined as:

$$S_w = \frac{\int_{A_i}^{A_0} U_\theta U_z r \; dA}{R_0 \int_{A_i}^{A_0} U_z^2 r \; dA} \tag{40}$$

where U_θ is the tangential component of the axial velocity, U_z is the axial velocity,

r is the radial distance from the center of the tube, and R_0 is the average radius

of the helically-finned tube. The integration feature of Fluent's postprocessor was

used to calculate both of the integrals in Equation (40). Swirl numbers were calculated at 0.10 m intervals along the axial direction of the long tube models. Furthermore, the percent difference between each consecutive swirl number was calculated. The swirling flow was expected to develop along the tube and become stable near the end of the tube. The swirl number along the long tube model of Case 5 is illustrated by the graph in Figure 6.4., which indicates that the swirl number converged near the end of the tube, where the percent difference between consecutive swirl numbers became virtually 0. Along with the fully developed velocity profile that was discussed in the last section, the converging swirl numbers along the Case 5 model strongly suggested that flow is fully developed near the end of the model. This verification process was repeated for each of the long tube models. The results were similar for each case.
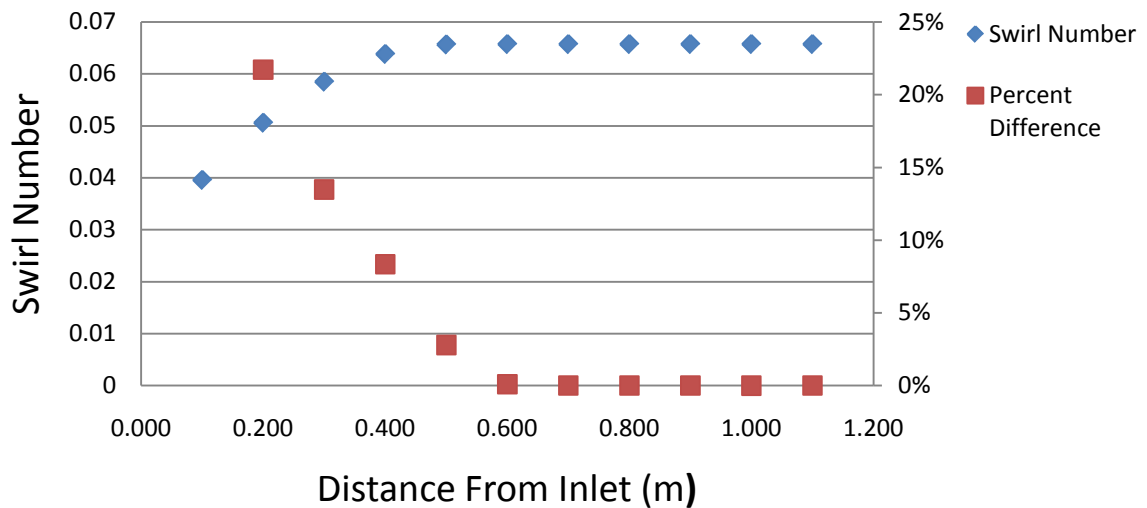

Figure 6.4.   Swirl Development along Case 5 – Long Tube Model.

Finally, the linear behavior of the numerical pressure drop along the axial center line of the long tube models was investigated. The pressure drop along each of the tube models was expected to be unstable near the inlet of each model. Near the exit, the pressure drop was expected to have become stable and linear. The pressure drop along the axial center line of the numerical model of Case 5 is illustrated in Figure 6.5., which shows that the pressure drop did become linear near the exit. This linear pressure drop was used to calculate the friction factor of the numerical fluid flow models. This investigation was performed for each of the long tube models, and each of the models exhibited similar stable linear pressure drops near the exits of the models.
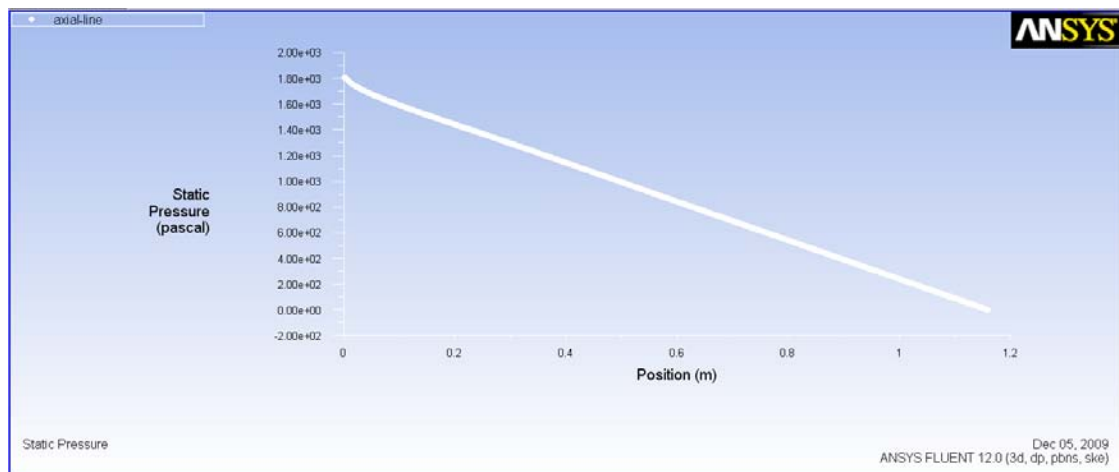

Figure 6.5.   Linear Pressure Drop along Case 5 – Long Tube Model.

Each of the 7 long tube models were scrutinized in the same fashion as previously described. The residual report of each model, the developing velocity field, the developing swirl number, and the pressure drop along each model were examined in order to verify that each model was satisfactorily solved and

complete. After examining the four solving factors of each case, all of the cases were determined to be acceptable models of the fluid flow within a helically-finned tube, and the Fluent solutions were used to determine the corresponding friction factor associated with each of the flow cases.

6.2.2 Convergence of the Mapping Models

In order to determine that the solution of each of the mapping models was complete, three solving factors were examined: the residual report, the velocity field along the tubular model, and the pressure drop along the model. Although seven mapping model flows were simulated, all of the solutions behaved similarly. Hence, only the solution factors of one of the cases are presented.

The residual report associated with Case 3 (mapping model) is illustrated in Figure 6.6. The cyclic and discontinuous graph lines of the residuals resulted from the looping process that was used to solve the sequence of models with Fluent. As presented in this figure, the residuals of the governing equations converged to at most 10^{-5} at the end of each cycle. Furthermore, the discontinuous spikes at the beginning of each successive cycle reduced in magnitude as Fluent resolved the model. The overall residuals appeared to stabilize as the solutions of the models were mapped and resolved. This suggests that the flow was becoming developed and repetitive. Each successive model became more similar to the fore-model, which was expected. Since the convergence criteria of the solution were satisfied, the convergence of residuals of the solution was considered to be satisfactory.
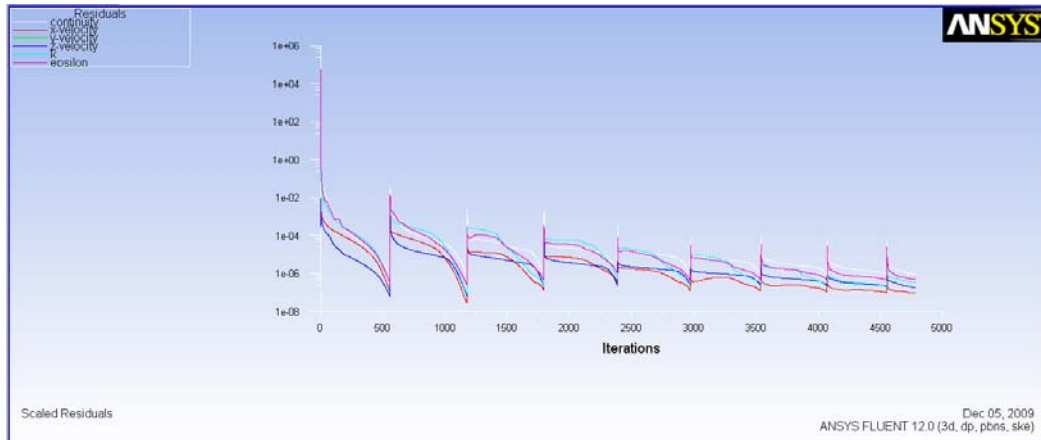
Figure 6.6.   Residual Report of Case 3 – Mapping Model.

The velocity field along the center planes of the mapping models was another solution factor that was considered. Only one rib-cycle of the helically-finned tube was modeled with the mapping modeling technique. The fluid flow developed over the repetitious looping process of solving the model in a sequential fashion. Thus, flow was expected to be fully developed in the model of the last loop. At the diameter of the model, the contours of the velocity field of Case 3 are illustrated in Figure 6.7. As expected, the magnitude of the velocity was greatest near the center of the tube and 0 m/s at the wall of the tube.
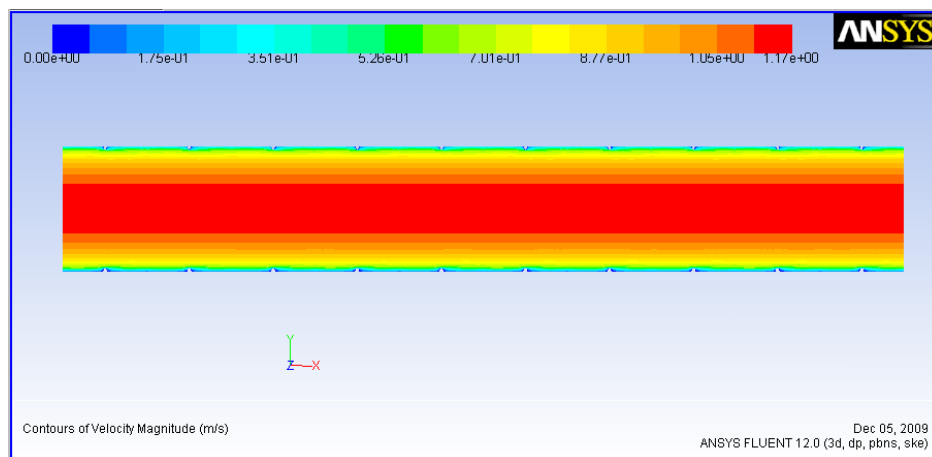

Figure 6.7.   Velocity Contours of Case 3 – Mapping Model.

Finally, the linear behavior of the pressure drop along the axial center line of each of the mapping models was investigated. The pressure drop along the numerical model in Case 3 is illustrated in Figure 6.8., which shows that the pressure drop is linear along the entire model. The linear pressure drop was used to calculate the friction factor associated with the numerical model. This type of investigation was performed for each of the mapping models. All of the models exhibited a similar linear pressure drop along the axial center line.
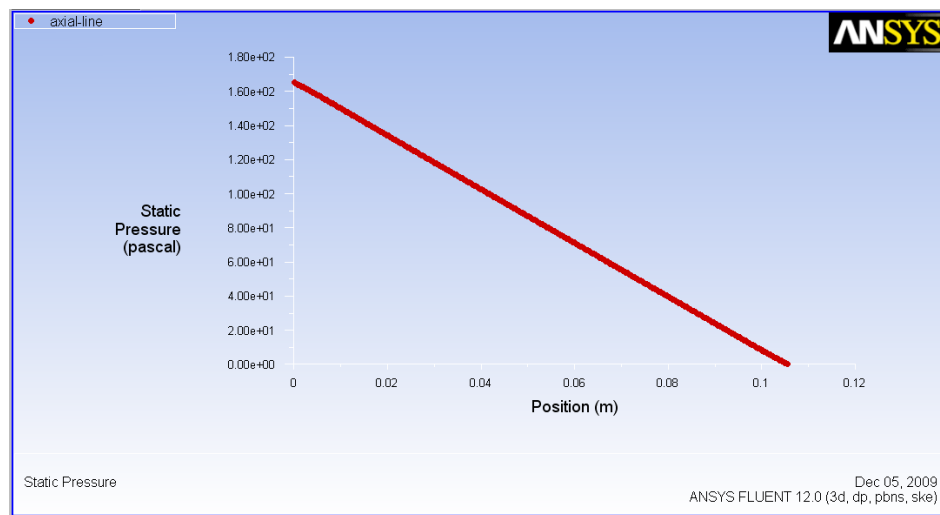

Figure 6.8.   Linear Pressure Drop along Case 3 – Mapping Model.

Each of the 7 mapping models was scrutinized in a similar fashion as previously outlined. The residual report of each model, the developing velocity field, and the pressure drop along each numerical model were examined in order to verify that the models were solved satisfactorily and completely. After each of the three solving factors had been examined, the simulations were all determined to be acceptable models of the fluid flow, and the numerical solutions were used to calculate the corresponding friction factor associated with each flow case.

6.2.3 Convergence of the Periodic Models

In order to determine that the solution of each of the periodic models was satisfactory, two solving factors were examined: the residual report, and the velocity field along the tubular model. Although seven periodic models were solved with Fluent, the solutions of each of the models behaved in a similar fashion with respect to the solving factors. Hence, only the solution factors of one case are presented.

The residual report of the periodic model of Case 2 is illustrated in Figure 6.9. Although the periodic model was iterated 6000 times, some of the residual values did not reduce to less than 10^{-1}. Moreover, the nearly flat shapes of the end-residual curves suggest that the convergence criteria would not have been satisfied for any reasonable or excessive number of iterations. Hence, the solution of the periodic model was suspect. Similar residual reports and convergence issues were observed for all of the periodic models.
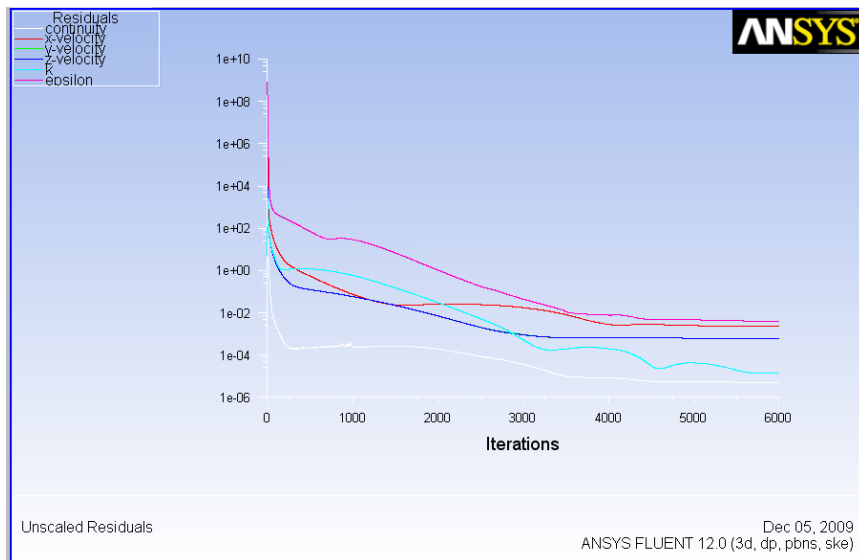

Figure 6.9.   Residual Report of Case 2 – Periodic Model.

The velocity field along the center plane of the periodic models was another solution factor that was considered. Similar to the mapping models, the periodic models consisted of only one rib-cycle of the helically-finned tube. However, there were no repetitious loops involved with the solving process; refer to Sections 4.4 and 5.2.3. Nevertheless, the velocity contours along the center plane of the periodic models were expected to be stable and fully developed. The velocity contours of Case 2 are illustrated in Figure 6.10. As expected, the magnitude of the velocity is greatest near the center of the tube and 0 m/s at the wall of the tube. However, the velocity profile is misshapen. The lower velocity contours shift downward toward the center portion of the model and back upward toward the end of the model. These velocity contours, illustrated in Figure 6.10, were unexpected. Similar results were observed in all of the solutions of the periodic models. Hence, the corresponding solutions were suspect.
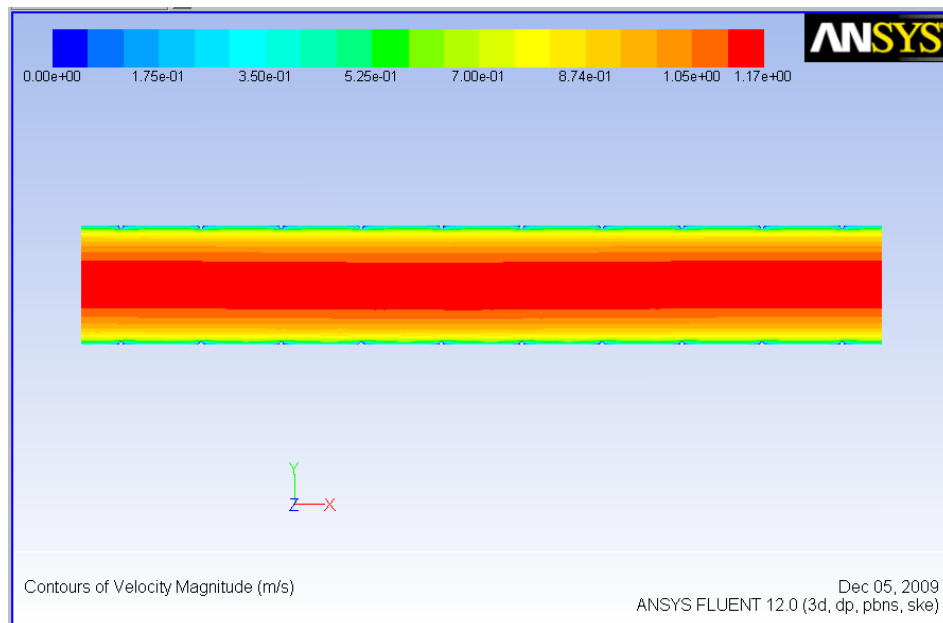

Figure 6.10.   Velocity Contours of Case 2 – Periodic Model.

Each of the periodic models was scrutinized in a similar fashion as previously described. The residual report of each model and the velocity contours along the axial direction of each model were examined in order to determine the completeness of the Fluent results. After the solving factors had been examined, all of the solutions contained unsatisfactory results. The residuals of each model did not satisfy the convergence criteria, and the velocity contours of each model were inconsistent. Therefore, the Fluent solutions associated with the periodic models were suspect. Nevertheless, the numerical pressure drop along each of the periodic models was obtained, and the corresponding friction factors were calculated.

6.2.4 Fluent Flow Friction Results

Using the Fluent solution of each flow case that was examined in this thesis, the corresponding friction factor was calculated using the pressure drop along the corresponding Fluent model. The friction factor was calculated three times for each case – one calculation for each case and each modeling technique. Thus, three friction factors were associated with each Fluent model. The friction factors were calculated using the common head loss equation, which is stated in Equation (41). The same equation was used by Zdaniuk et al. (2008) to calculate the experimental friction factors.

$$f = \frac{2\Delta P D}{\Delta x \rho V^2} \tag{41}$$

where ΔP is the pressure drop along the model, D is the nominal diameter of the helically-finned tube, Δx is the length over which ΔP is measured, ρ is the density of water, and V is the average velocity of the flow within the tube.

The experimental friction data that was obtained by Zdaniuk et al. (2008), along with the corresponding velocities that were observed in the experiment, are listed in Table 6.3. The corresponding case identification names that were used by Zdaniuk et al. (2008) are displayed in Table 5.1. The velocities that were reported in Zdaniuk et al. (2008) were used in the Fluent flow models. Notice the relationship between the experimental friction factors and the corresponding velocities. As the velocities increased, the friction factors decreased. In order to determine the success of the Fluent models and the friction factors, the numerical data was compared to the experimental data.

Table 6.3   Experimental Flow Data from Zdaniuk et al. (2008).

Case Number	Friction Factor	Velocity (m/s)
1	0.012370	0.886
2	0.011399	1.353
3	0.010508	1.773
4	0.010084	2.167
5	0.009598	2.636
6	0.009061	3.227
7	0.008505	3.949

Using the numerical solution data of each of the Fluent models in conjunction with Equation (41), the three friction factors of each of the flow cases

were calculated. The resulting friction factors, along with the experimental friction

factors, are presented in Table 6.4.

Table 6.4   Numerical Friction Data and Experimental Friction Data.

Case Number	Friction Factor From Fluent Model			Experimental Friction Factor [Zdaniuk et al. (2008)]
	Long Tube Model	Mapping Model	Periodic Model	
1	0.01502	0.01566	0.01559	0.01237
2	0.01341	0.01403	0.01400	0.01140
3	0.01245	0.01303	0.01301	0.01051
4	0.01171	0.01231	0.01230	0.01008
5	0.01105	0.01161	0.01159	0.00960
6	0.01038	0.01091	0.01090	0.00906
7	0.00978	0.01021	0.01029	0.00851

In order to better visualize the numerical data verses the experimental data, all

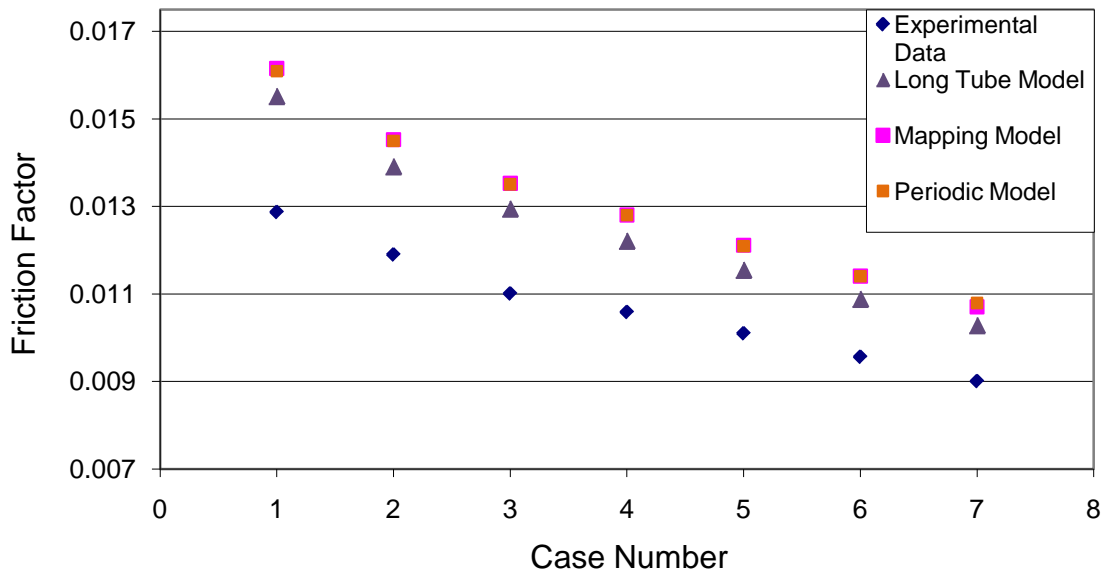four sets of data are juxtaposed in Figure 6.11.

Figure 6.11. Numerical Friction Results *vs.* Experimental Friction Results.

From Figure 6.11, there are clearly similarities and different between the data sets. One of the most conspicuous similarities is the downward trend of each data set. The friction factors, regardless of the modeling technique, exhibit the same downward trend as the velocities were increased. Another similarity among the data sets is the close agreement between the mapping modeling technique and the periodic modeling technique. From Figure 6.11, the numerical friction data from each of the Fluent modeling techniques appear to closely agree with one another. However, there are stark agreements and disagreements among the data sets, too. Namely, the numerical friction factors are greater than the experimental friction factors, and the Fluent data points are more closely in agreement with one another than the experimental data. In order to illustrate the deviations of the numerical friction factors relative to the experimental friction factors, the percent error was calculated using Equation (42).

$$\% \ Error = \frac{\left| f_{exp} - f_{fl} \right|}{f_{exp}} \tag{42}$$

With respect to the corresponding experimental friction factor, the percent errors associated with all of the numerical friction results are displayed in Table 6.5. The percent error of the numerical friction results ranged from 14.6% to 26.6%. From Table 6.5, it is clear that the long tube model results more closely agreed with the experimental friction data than the mapping model results or periodic model results. Figure 6.12 shows the percent errors of the numerical friction results with respect to the modeling techniques. As illustrated by the Figure 6.12, the percent

91

error of the numerical friction factors for all three techniques decreased, spiked, and gradually leveled off as the velocity in each consecutive case was increased. Table 6.3 displays the respective average velocity of each case.

Table 6.5   Percent Error of Numerical Friction Factors.

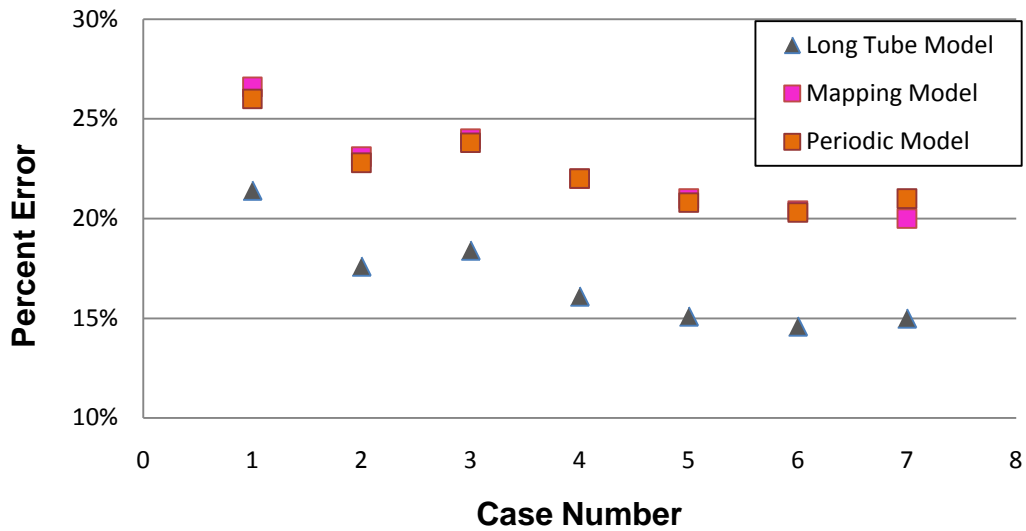| Percent Error		
Long Tube Model	Mapping	Periodic BC
21.4%	26.6%	26.0%
17.6%	23.1%	22.8%
18.4%	24.0%	23.8%
16.1%	22.0%	22.0%
15.1%	21.0%	20.8%
14.6%	20.4%	20.3%
15.0%	20.0%	21.0%

Figure 6.12. Percent Error with Respect to Modeling Techniques.

6.3 <u>Recommendations and Future Work</u>

The primary objective of this research was to successfully model the flow within a helically-finned tube, compare the simulation results to the experimental results, and investigate the performance of three distinct modeling techniques that were used to simulate the fluid flow. Although the objective was achieved and satisfactory results were obtained, the measure of success of this endeavor is arguably subjective. Nevertheless, there were several observations that presented during this thesis, and these observations are worth mentioning.

As discussed in Chapter 5, some of the information regarding the experimental setup and data from Zdaniuk et al. (2008) was limited, as several key parameters were unknown. Specifically, the roughness height of the inner surface of the experimental tubes, the quality of the rib fins, and the accuracy of the rib measurements were not mentioned in the report. As communicated from Gregory Zdaniuk to the author of this thesis by email, such qualities were neither measured nor considered. As pointed out in several highlighted articles from Section 1.2, Literature Review, the intricate parameters of the tube and rib geometries greatly affect the friction performance of an enhanced tube. Thus, the discrepancies that were observed between the Fluent data and experimental data possibly resulted from the overlooked measurements or unknown qualities of the experimental tubes. Of course, the unknown information was left out of the Fluent models, but the effects of such were inherently, and unknowingly, incorporated in the experimental results. Hence, error was expected. One way to abate this problem is to personally perform the helically-finned tube experiment,

examine all of the pertinent features of the tubes, and incorporate all of the information in the analysis.

The use of the periodic model for the flow within the tubes that was considered in this thesis is another concern. As discussed in Section 4.4, the basic assumption of the periodic boundary conditions is that the fluid flow between the periodic boundaries repeats with respect to velocity and position. However, as Jensen and Vlakancic (1999) pointed out, the fluid within a helically finned tube does not always follow the helical pattern of the ribs exactly. The flow within helical tubes has been observed 'jumping' the ribs and swirling at a different helical period than that of the ribs. Jensen and Vlakancic (1999) reported that the degree to which a flow follows the pattern of the ribs is a function of helix angle, fin height, velocity, and rib number. As a result of considering only one rib cycle in the periodic models, the basic assumption of the model may not have been satisfied, as the helical period of the physical flow was different from the period of the helical ribs that lay between the periodic boundaries. One way to investigate the effectiveness of the periodic boundary conditions is to model a helically-finned tube within which the flow is known to strictly follow the periodic nature of the helical ribs. After obtaining a numerical solution, the residual report and the velocity contours should be scrutinized for evidence of the same inconsistencies that were observed in this thesis. Lastly, the numerical friction factor should be compared to existing experimental data.

An important concept that was overlooked and not incorporated into this thesis is grid convergence analysis. The purpose of this analysis is to determine

the minimum number of mesh elements that are required of a model in order to achieve satisfactory results, as opposed to using a superfluous amount of elements. Using more mesh elements than that which is necessary is computationally inefficient. For example, two models, M1 and M2, are identical in every way except for the number of mesh elements that comprise each model. M1 consists of 2 million elements and M2 consists of 1 million elements. It is possible that both models yield similar solutions, yet the M1 is significantly more expensive computationally. Clearly, M2 is the better model. With respect to this thesis, grid convergence was not incorporated into the construction of meshed models. However, there is the possibility that the numerical results of this thesis could have been obtained with leaner models. Consequently, the computing time and the required computing resources would have been reduced.

As for future work, there are many opportunities available. Some of the research that was presented in Section 1.2, Literature Review, suggests that the friction factor of a helically-finned tube is significantly influenced by several tube parameters. A helically-finned tube that is highly desirable is one that is optimized for high swirl flow and low friction. Such can be investigated with Fluent by considering various tube configurations and simulating the flows. The friction factor and swirl flow can be determined from the numerical data using the methods presented in this thesis.

Another possibility is to investigate the heat transfer characteristics of the helically finned tube as a function of tube parameters. Fluent is fully capable of coupling heat transfer and fluid flow. As discussed in Section 1.2, there is an

intimate relationship between the geometric parameters and the heat transfer performance of an enhanced tube. This relationship can be investigated by using Fluent to simulate the heat transfer characteristics of a tube. Currently, research concerning helically-finned tubes is directed toward the discovery of a closed model of the fluid flow, friction, and heat transfer performance of the tubes.

Although this research successfully simulated the flow within a helically-finned tube and corroborated the friction factors that were determined experimentally, there is still the possibility of improving the simulation process that was used, and multiple directions for further research exist.

REFERENCES

Belyakov, I. I., V. K. Migai, and V.V. Sokolov. "Heat Transfer and Hydraulic Resistance of Tubes with Internal Helical Finning." <u>Thermal Engineering</u>. 36 (1989) : 444-448

Çengel, Y. A., and Boles, M.A. *Thermodynamics: An Engineering Approach*. 6th ed. Boston: McGraw Hill, 2006.

Energy Information Administration (EIA), "Electricity Explained: Electricity in the United States." 16 July. 2009. http://tonto.eia.doe.gov/energyexplained/index.cfm?page=electricity_in_the_united_states

Fluent Inc. "Fluent User's Guide." Fluent Version 12, Fluent Inc., 2006.

Fox, Robert W., Alan T. McDonald, and Philip J. Pritchard. *Introduction to Fluid Mechanics.* 6th ed. John Wiley & Sons, Inc., 2004

Jensen, M.K., and A. Vlakancic. "Experimental Investigation of Turbulent Heat Transfer and Fluid Flow in Internally Finned Tubes." <u>International Journal of Heat and Mass Transfer</u>. 42 (1999) : 1343-1351.

Stultz, S.C. *Steam: Its Generation and Use.* 41st ed. Barberton, Ohio: The Babcock & Wilcox Company, 2005.

Webb, R.L. "Performance, Cost Effectiveness, and Water-side Fouling Considerations of Enhanced Tube Heat Exchangers for Boiling Services with Tube-Side Water Flow." <u>Heat Transfer Engineering</u>. 3 (1984) : 84-98.

Webb, R. L., R. Narayanamurthy, and P. Thors. "Heat Transfer and Friction Characteristics of Internal Helical-Rib Roughness." <u>Transactions of the ASME: Journal of Heat Transfer</u>, 122 (2000) : 134-142.

Zdaniuk, Gregory. "Heat Transfer and Friction in Helically-Finned Tubes Using Artificial Neural Networks." Diss. Mississippi State, 2006.

Zdaniuk, Gregory, J., Louay M. Chamra, and Pedro J. Mago. "Experimental Determination of Heat Transfer and Friction in Helically-Finned Tubes." <u>Experimental Thermal and Fluid Science</u>. 32 (2008) : 761-775

APPENDIX A

JOURNAL FILES

A.1 Journal File for Long Tube Model

```
file
read-case-data
/nm/users/mja/jls/thesis/multicycletube/1p5e6/multicycle1p5e6.0.cas
yes
q

solve
iterate
1500
q

file
write-case-data
/nm/users/mja/jls/thesis/multicycletube/1p5e6/multicycle1p5e6.1.cas
yes
q

q
q

exit
yes
```

A.2   Journal File for Short Tube Mapping Method

Run 1:

```
file
read-case-data
/nm/users/mja/jls/thesis/1cyclemapping/C3/1CycMapC3.0.cas
y
q

solve
iterate
600
q

file
write-case-data
/nm/users/mja/jls/thesis/1cyclemapping/C3/1CycMapC3.1.cas
y

q
q

exit
yes
```

Run 2:

```
file
read-case-data
/nm/users/mja/jls/thesis/1cyclemapping/C1/1CycMapC1.1.cas
q

solve
monitors
residual
check-convergence?
n
n
n
n
n
n
q
q
q

solve
```

iterate
4
q

solve
monitors
residual
check-convergence?
y
y
y
y
y
y
q
q
q

solve
iterate
650

q

file
write-profile
/nm/users/mja/jls/thesis/1cyclemapping/C1/outflow.prof
y
**** outflow

x-velocity
y-velocity
z-velocity
turb-diss-rate
turb-kinetic-energy
/
read-profile
/nm/users/mja/jls/thesis/1cyclemapping/C1/outflow.prof
q
define
boundary-conditions
velocity-inlet
inlet
n
y
y
y
y
y
y
y

```
y
y
y
y
y
y
y
q
q

solve
initialize
compute-defaults
velocity-inlet
inlet
q
q
q

solve
monitors
residual
check-convergence?
n
n
n
n
n
n
q
q
q

solve
iterate
3
q

solve
monitors
residual
check-convergence?
y
y
y
y
y
y
q
q
q
```

```
solve
iterate
650

q

file
write-profile
/nm/users/mja/jls/thesis/1cyclemapping/C1/outflow.prof
```
****   y

Note: Here, the sequence of code between the ****'s repeats seven more times and continues with the following lines of code.

```
q

q
q

exit
yes
```

A.3 Journal File for Short Tube Periodic Method

```
file
read-case-data
/nm/users/mja/jls/thesis/1cycleperiodic/C5/1CycPerC5.cas
y
q

solve
iterate
6000
q

file
write-case-data
/nm/users/mja/jls/thesis/1cycleperiodic/C5/1CycPerC5.1.cas
y
q

q
q

exit
yes
```